Generating ~~Large~~large-scale sea ice motion from Sentinel-1 and the RADARSAT Constellation Mission using the Environment and Climate Change Canada automated sea ice tracking system

Stephen E.L. Howell[1], Mike Brady[1] and Alexander S. Komarov[2]

[1]Climate Research Division, Environment and Climate Change Canada, Toronto, Canada
[2]Meteorological Research Division, Environment and Climate Change Canada, Ottawa, Canada

Correspondence to: Stephen E.L. Howell (Stephen.Howell@ec.gc.ca)

Abstract. As Arctic sea ice extent continues to decline, remote sensing observations are becoming even more vital for the monitoring and understanding of sea ice. Recently, the sea ice community has entered a new era of synthetic aperture radar (SAR) satellites operating at C-band with the launch of Sentinel-1A in 2014, Sentinel-1B in 2016 and the RADARSAT Constellation Mission (RCM) in 2019. These missions represent 5 spaceborne SAR sensors, that together routinely cover the pan-Arctic sea ice domain. Here, we describe, apply and validate the Environment and Climate Change Canada automated sea ice tracking system (ECCC-ASITS) that routinely generates large-scale sea ice motion (SIM) over the pan-Arctic domain using SAR images from S1 and RCM. We applied the ECCC-ASITS to the incoming image streams of S1 and RCM from March 2020 to October 2021 using a total of 135,471 SAR images and generated new SIM datasets (7-day 25 km and 3-day 6.25 km) by combining the image stream outputs of S1 and RCM (S1+RCM). Results indicate that S1+RCM SIM provides more coverage in Hudson Bay, Davis Strait, Beaufort Sea, Bering Sea, and directly over the North Pole compared to SIM from S1 alone. Based on the resolvable S1+RCM SIM grid cells, the 7-day 25 km spatiotemporal scale is able to provide the most complete picture of SIM across the pan-Arctic from SAR imagery alone but considerable spatiotemporal coverage is also available from 3-day 6.25 products. S1+RCM SIM is resolved within the narrow channels and inlets of the Canadian Arctic Archipelago filling a major gap from coarser resolution sensors. Validating the ECCC-ASITS using S1 and RCM imagery against buoys indicate a root mean square error (RMSE) of 2.78 km for dry ice conditions and 3.43 km for melt season conditions. Larger speeds are more apparent with S1+RCM SIM as comparison with the National Snow and Ice Data Center (NSIDC) SIM product and the Ocean and Sea Ice Satellite Application Facility (OSI SAF) SIM product indicated a RMSE of u=4.6 km/day and v=4.7 km/day for the NSIDC and u=3.9 km/day and v=3.9 km/day for OSI-SAF. Overall, our results demonstrate the robustness of the ECCC-ASITS for routinely generating large-scale SIM entirely from SAR imagery across the pan-Arctic domain.

~~Here, we utilized over 60,000 SAR images from Sentinel-1AB (S1) and RCM to generate large-scale sea ice motion (SIM) estimates over the pan-Arctic domain from March to December, 2020. On average, 4.5 million SIM vectors from S1 and RCM were automatically detected per week for 2020 and when combined (S1+RCM) they facilitated the generation of 7-day, 25 km SIM products across the pan-Arctic domain. S1+RCM SIM provided more coverage in Hudson Bay, Davis Strait, Beaufort Sea, Bering Sea, and over the North Pole compared to SIM from S1 alone. S1+RCM SIM was able to be resolved within the~~

~~narrow channels and inlets across the pan-Arctic alleviating the main limitation of coarser resolution sensors. S1+RCM SIM provided larger ice speeds with a mean difference (MD) of 1.3 km/day compared to the National Snow and Ice Data Center (NSIDC) SIM product and a MD of 0.76 km/day compared to Ocean and Sea Ice Satellite Application Facility (OSI-SAF) SIM product. S1+RCM was also able to better resolve SIM in the marginal ice zone compared to the NSIDC and OSA-SAF SIM products. Overall, our results demonstrate that combining SIM from multiple spaceborne SAR satellites allows for large-scale SIM to be routinely generated across the pan-Arctic domain.~~

1 Introduction

As Arctic sea ice extent continues to decline in concert with increases in carbon dioxide (CO_2) emissions (Notz and Stroeve, 2016), remote sensing observations are becoming even more vital for the monitoring and understanding of Arctic sea ice. Recently, the sea ice community has entered a new era of synthetic aperture radar (SAR) satellites operating at C-band (wavelength, λ = 5.5 cm) with the launch of Sentinel-1A in 2014, Sentinel-1B in 2016 (S1; Tores et al., 2012) and the RADARSAT Constellation Mission (RCM) in 2019 (Thompson, 2015). Together these missions represent 5 spaceborne SAR sensors that when combined offer the opportunity to retrieve large-scale sea ice geophysical variables with high spatiotemporal resolution. ~~Small et al. (2021) demonstrated that combining SAR images from S1 and RADARSAT-2 allowed for the production of high spatiotemporal resolution analysis-ready composite products for large regions. Howell et al. (2019) used analysis-ready composite products generated from S1 and RADARSAT-2 based on the approach described by Small et al., (2021) to provide high spatial resolution estimates of melt onset over a large region in the northern Canadian Arctic.~~ An important sea ice geophysical variable that could also benefit from large-scale SAR estimates across the Arctic is sea ice motion (SIM). SIM is controlled by the exchange of momentum due to turbulent process primarily from atmospheric and oceanic forcing. Away from the coast, winds explain 70% or more of the variance in Arctic sea ice motion (Thorndike and Colony, 1982) and as a result, monitoring changes in SIM is important for understanding how sea ice responds to changes in atmospheric circulation (Rigor et al., 2002). SIM convergent and divergent processes impact the overall thickness of Arctic sea ice (Kwok, 2015) and the dynamic component of the Arctic sea ice area and volume balance is also impacted by SIM (Kwok, 2004; Kwok, 2009). The long-term record of SIM in the Arctic indicates the ice speed is increasing which are associated with thinner ice being more susceptible to wind forcing (Rampal et al., 2007; Kwok et al., 2013; Moore et al., 2019).

Techniques for estimating SIM from satellite observations have a long history dating back to the late 1980s and early 1990s that are primarily based on the maximum cross-correlation coefficient between overlapping images (e.g. Fily and Rothrock, 1987; Kwok et al., 1990; Emery et al., 1991). The maximum cross-correlation approach to estimate SIM can be applied to virtually any overlapping pair of satellite imagery separated by a relatively short time interval of ~1-3 days. For large-scale SIM, passive microwave imagery is typically the most widely used because of its large swath and daily coverage (e.g. Agnew et al., 1997; Kwok et al., 1998; Lavergne et al., 2010; Tschudi et al., 2020). Enhanced resolution SIM products with spatial resolutions of ~2 km have also been generated (e.g. Haarpaintner, 2006; Agnew et al., 2008) although they have not been widely utilized. The limitation~~trade-off~~ with respect to large-scale SIM estimated from passive microwave imagery, however, is a low spatial resolution (~~12-25~~50-100 km). As a result, SIM is more difficult to track with lower spatial resolution passive microwave sensors (Kwok et al., 1998) especially, within narrow channels and inlets (e.g. the Canadian Arctic Archipelago; CAA) compared to SAR. However, SIM estimates from SAR are typically regionally based because of image availability across the Arctic. With the availability of SAR imagery from S1 and RCM, a new opportunity exists to provide both the operational and scientific communities with larger-scale estimates of SIM from SAR. In addition, with marine activity in the Arctic increasing (e.g. Eguíluz et al., 2016, Dawson et al., 2018), a wide-range of maritime stakeholders could benefit from access to large-scale SAR SIM for safety, planning and situational awareness (Wagner et al., 2020).

In this study, we describe, apply, and validate the Environment and Climate Change Canada automated sea ice tracking system (ECCC-ASITS) using SAR imagery from the S1 and RCM to generate new SIM products over the pan-Arctic domain. ~~In this study we make use of 5 SAR satellites from the S1 and RCM missions to generate SIM over the large-scale pan-Arctic domain (Fig. 1).~~ To our knowledge this is perhaps the first time such an extensive ~~combining~~ processing of SAR imagery at the pan-Arctic scale has been undertaken to generate SIM. The ECCC-ASTIS is designed to facilitate the routine generation of SIM to serve operations within ECCC and provide new and unique SIM data to the wider scientific community and maritime stakeholders. Here, w~~W~~e focus primarily on the latter applications by first describ~~e~~ing ~~our~~ the ECCC-ASITS ~~work flow that~~workflow that estimates SIM from S1 and RCM SAR imagery (hereafter, S1+RCM) in close to near-real time and combines the output into ~~a~~ S1+RCM SIM products. We then present the results of two S1+RCM products from March 2020 to October 2021 followed by a ~~then discuss~~ section discussing the validation and uncertainty of S1+RCM SIM products. ~~the vector quality and SIM uncertainty of large-scale of the S1+RCM SIM over the annual cycle for the Arctic and its sub-regions.~~ Finally, we provide a detailed compareison of our S1+RCM SIM ~~estimates~~ product to the existing SIM datasets from the National Snow and Ice Data Center (NSIDC) (Tschudi et al., 2020) and Ocean and Sea Ice-Satellite Application Facility (OSI-SAF) SIM ~~(OSI-SAF)~~ (Lavergne et al., 2010).

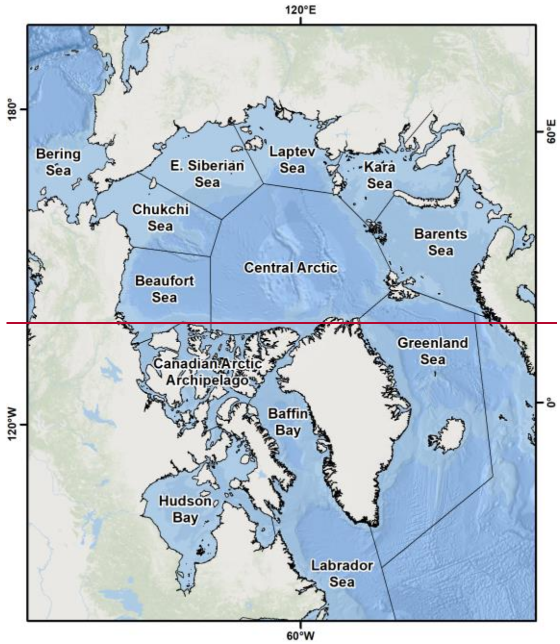

~~**Figure 1. Study area domain including sub-regions.**~~

2 Data

The primary datasets used in this analysis were Extra Wide Swath imagery at HH polarization from S1 and ScanSAR 50 m (SC50M), ScanSAR 100 m (SC100M), and ScanSAR Low Noise (SCLN) at HH polarization from RCM from March 2020 to ~~December 2020~~October 31, 2021 (Table 1). ~~With the recent availability of RCM imagery in 2020, this provided an additional 29,744 images that when combined with S1 (~32,810 images) resulted in 60,000+ images being available to generate SIM across the pan-Arctic for 2020.~~We also used daily buoy positions from International Arctic Buoy Programme (IABP) for April and August 2020 and 2021, 7-day SIM NSIDC Polar Pathfinder dataset and the 2-day- multi-sensor low resolution 62.5 km~~the 2-day~~ OSI-SAF sea ice motion dataset (OSI-405) from March to December 2020. Tschudi et al., (2020) provides a complete description of the NSIDC Polar Pathfinder SIM dataset, and Lavergne et al., (2010) provides a complete description of the OSI-SAF SIM dataset. Finally, we used ~~the 2020~~ daily pan-Arctic ice charts from the National Ice Center for 2020 and 2021~~.~~

Table 1. Satellite SAR image inventory used in this analysis from March 2020 to October 2021. ~~December 2020.~~

Platform	Beam Mode	Pixel Size (m)	Swath (km)	Image Count
RCM	Single Beam Medium Resolution (SC16M)	6.25	30	123
	ScanSAR Medium Resolution (SC30M)	12.5	125	115
	ScanSAR Medium Resolution 50 m (SC50M)	20	350	50,468
	Scan SAR Low Resolution 100 m (SC100M)	40	500	18,384
	ScanSAR Low Noise (SCLN)	40	350	1,857
S1	Extra-Wide Swath (EW)	40	410	64,524

3 Methods

3.1 ECCC a~~A~~utomated sea ice ~~motion~~ tracking algorithm

We make use of the automated SIM tracking algorithm developed by Komarov and Barber (2014) to estimate large-scale SIM across the pan-Arctic domain. The algorithm has been widely utilized for applications that require robust estimates of SIM in Arctic using SAR at C-band (e.g. Howell et al., 2013; Howell et al., 2018; Komarov and Buehner, 2019; Moore et al., 2021a). A full description is provided by Komarov and Barber (2014), but the main components of the algorithm are briefly described here. To begin with, coarser spatial resolution ~~levels~~ images are generated from the original spatial resolution of the SAR image pairs. For example, if the original SAR image pairs have a spatial resolution of 200 m then the additional generated levels would be 400 m and 800 m. A set of control points (i.e.~~,~~ ice features) is automatically generated for each resolution level based on the SAR image local variances. To highlight edges and heterogeneities at each resolution level, a Gaussian filter and the Laplace operator are applied sequentially. Beginning with the coarsest~~lowest~~ resolution level, ice feature matches in the image pairs are identified by combining the phase-correlation and cross-correlation matching techniques that allows for both the translation and rotational components of SIM to be identified. SIM vectors not presented in both forward and backwards image registration passes are filtered out, as well as vectors with low cross-correlation coefficients. In order to refine the SIM vectors, at each consecutive resolution level the algorithm is guided by SIM vectors identified at the previous resolution. An example of the SIM output generated from the algorithm based on two overlapping SAR image is shown in Fig. ~~2~~1. The limitations that are widely known with respect to estimating SIM from SAR imagery include regions of low ice concentration, melt water on the surface of the sea ice and longer time separation between images also apply to this algorithm.

~~The algorithm has been widely utilized for applications that require robust estimates of SIM in Arctic using SAR at C-band (e.g. Howell et al., 2013; Howell et al., 2018; Komarov and Buehner, 2019; Moore et al., 2021). Moreover, when the SIM vector outputs were collocated and coincided with ice buoy trajectories, it was found to have a root-mean square error (RMSE) of 0.43 km. The limitations that are widely known with respect to estimating SIM from SAR imagery include regions of low ice concentration, melt water on the surface of the sea ice and longer time separation between images also apply to this algorithm.~~

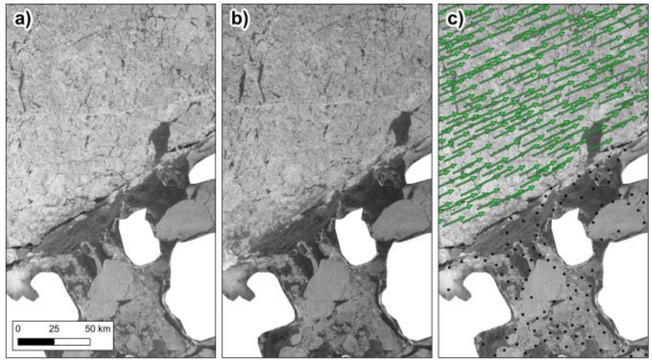

Figure ~~2~~1. a) RCM image on April 7, 2020, b) RCM image on April 10, 2020, and c) detected sea ice motion vectors (green) over RCM April 7, 2020. The black dotes indicate detection vectors with no motion. RADARSAT Constellation Mission Imagery © Government of Canada 2020. RADARSAT is an official mark of the Canadian Space Agency.

3.2 ~~Generating large-scale gridded sea ice motion~~ECCC automated sea ice motion tracking system (ECCC-ASITS)

The ECCC-ASTIS facilitates the routine generation of S1+RCM SIM products however, it should be noted the system has roots (i.e. built-up) in previous studies (e.g. Howell and Brady, 2019; Moore et al., 2021a; Moore et al., 2021b). While the primary system methodology described here is for larger-scale SIM generation, it is not strictly limited for this application and can (has) been modified to accommodate research or operational specific objectives.

The generalized processing chain for generating large-scale S1+RCM SIM using ECCC-ASTIS is illustrated in Fig. ~~3~~2. The approach processes the S1 and RCM image streams separately and then combines the outputs into a S1+RCM SIM product. This parallel approach was chosen for several reasons. First, mixing S1 and RCM primarily improves spatial coverage as RCM mainly fills in the spatial gaps in S1 coverage as RCM coverage is more widely spread across the Arctic and covering Bering Sea, Laptev Sea, Davis Strait, Southern Beaufort Sea and even the North Pole thus filling a gap typically associated with the majority of satellite sensors (Fig. 3). An example of the ability of RCM to almost completely cover the North Pole on a single day is shown in Fig. 4. However, we note that the temporal resolution of SIM could be improved by mixing S1 and RCM but this would be restricted to only certain regions of the Arctic. Second, ~~because~~ SAR imagery is received by ~~Environment and Climate Change Canada (~~ECCC~~)~~ from S1 and RCM in close to near-real time and in order to “keep-up” with the 100’s of images coming in per day and routinely generate products every day ~~and the subsequent computational load on automated SIM detection,~~ the processing system is run every hour given computational load on automated SIM detection,. Fig 5. illustrates the amount of S1 and RCM SAR imagery that was processed over a 7-day time period in March 2020 which amounted to over 1132 SAR images or ~160 images per day. ~~As a result~~Finally, ~~, S1 and RCM imagery are currently not mixed together for automated SIM tracking given the~~ the different orbit characteristics of the satellites which contribute to differences in terms of when images are acquired compared to when they are received by ECCC. For example, if an S1 image acquired at 1300h UTC is transferred to our system sooner than an RCM image that was acquired at 1100h UTC then the RCM image would be missed. We note that S1A and S1B are freely mixed in the Sentinel processing chain as well as RCM1, RCM2 and RCM3 are mixed in the RCM processing chain.

For both S1 and RCM images streams, the pre-processing steps shown in Fig. ~~3~~ 2 first involve calibrating the imagery to the backscatter coefficient of sigma nought (σ°) using the HH-polarization channel and map-projected to the NSIDC North Pole Stereographic WGS-84, EPSG:3413 coordinate system with a 200 m pixel size. For S1 imagery, pre-processing steps were applied using the Graph Processing Tool (GPT) of the Sentinel Application Platform (SNAP) software, and for RCM imagery, the pre-processing workflow was applied using an in-house pre-processor.

Manual inspection of SAR imagery and subsequent image stack compilation prior to automatic SIM generation, while effective in regional-scale studies (e.g. Howell et al., 2013; Howell et al., 2016; Moore et al., 2021) is not practical for generating large-scale SIM. The main challenges of estimating large-scale SIM across the pan-Arctic domain are (i) handling the large volume and delivery frequency of the imagery, (ii) efficiently selecting image stacks, and (iii) providing more computationally efficient feature tracking from the image stacks.

To address (i) and (ii), an automated approach for determining the suitability of images for inclusion in the automatic SIM generation (i.e. S1 or RCM image stack selection) was developed and depicted in Fig. ~~3~~6. For the image stack selection, a 400 km x 400 km grid of sectors encompassing the pan-Arctic was generated and used to create overlapping stacks of SAR image pairs (Fig. 6) ~~(Fig. 3)~~. The footprint geometry of each SAR image was compared to a given sector's extent and if the overlap <= 30% was achieved, that image was retained for feature tracking. Next, we assess image-to-image overlap within each sector to create a temporally sequential image stack that intersected one another to an acceptable degree (>=32,000 km^2). Images within each sector with an overlap of at least 32,000 km^2 were retained for feature tracking. The stacks are created every hour using the last-processed image from the previous run and the accumulated new imagery that had arrived in the time preceding.

For (iii), a more computationally efficient application of automatic SIM tracking algorithm (i.e. image stack processing) was developed. Traditionally, image stacks were processed serially which was effective for local-scale studies with limited amounts of imagery, but with significant increases in the SAR image data volume and study area domain size from S1 and RCM, it was necessary to enhance the processing speed of ice feature tracking analysis. The concurrent approach as outlined in Fig. ~~5~~ 7 takes advantage of vertical scalability by increasing the number of processes during image pair analysis. This approach allowed for an entire image stack to be efficiently processed with as many computational cores as were available. For example, when three sets of image pairs are processing and process 3 finishes before process 2, process 3 picks up the next sequence of pairs instead of waiting for process 2 (Fig. ~~5~~7). After stack processing, the last-processed image for the given sector is recorded in a database and processing ends. It is important to note there is currently no "staleness" limit for the SAR images in a given sector. There are occasionally instances when long stretches of time (e.g. 7-days) occur between images pairs but this is mostly confined to the edge-sectors of the grid. Unfortunately, the computational capacity to take on the additional processing load of using the same image in multiple pair combinations is not currently available in the infrastructure being used.

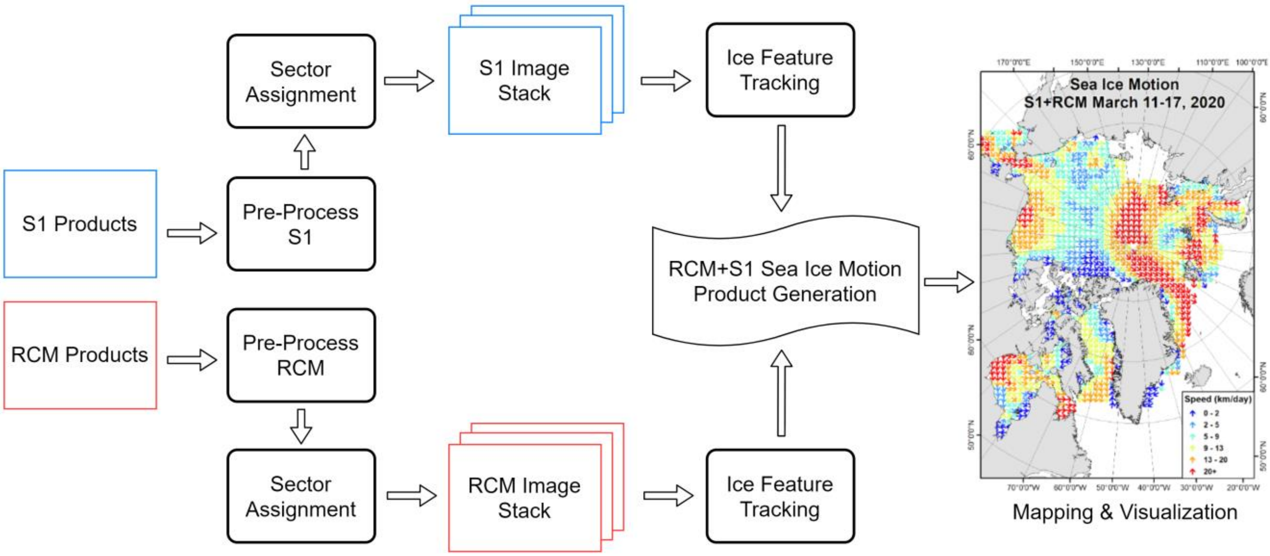

Figure ~~3~~2. Generalized processing chain for generating large-scale sea ice motion from S1 and RCM across the pan-Arctic domain.

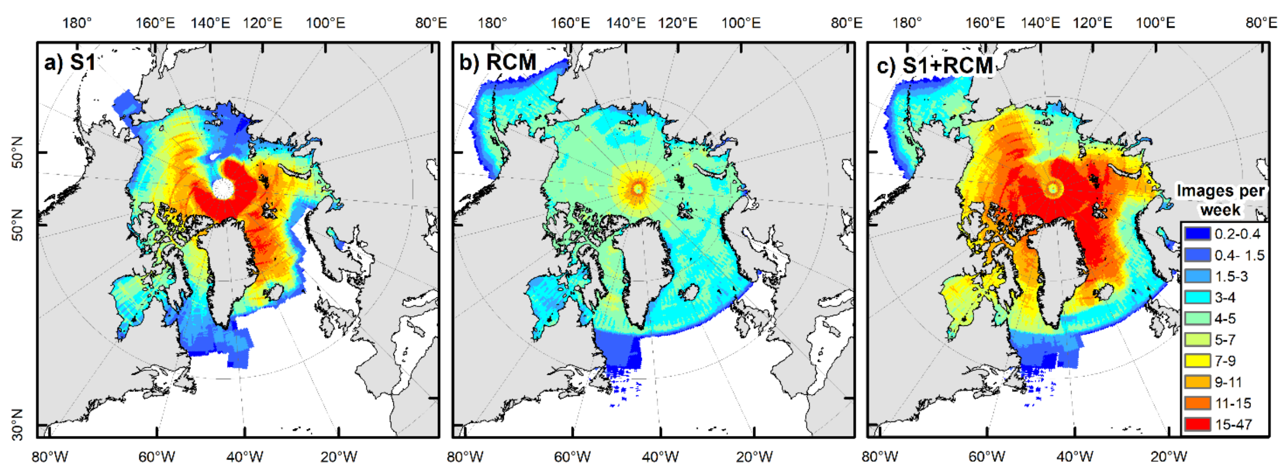

Figure 3. Image density per week for a) S1, b) RCM, and c) S1+RCM based on Table 1

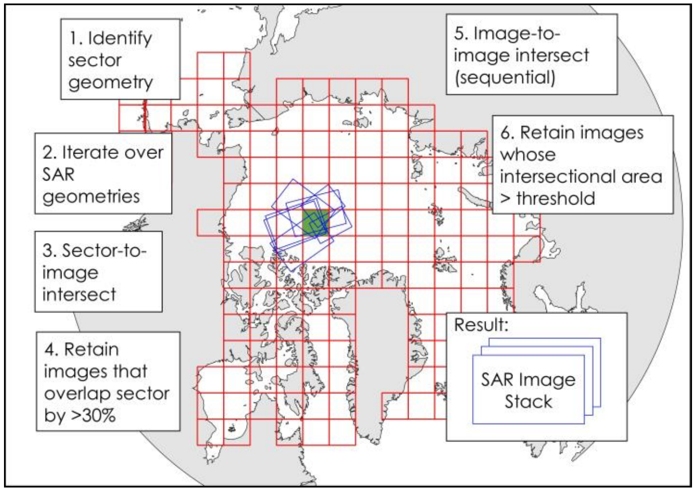

Figure ~~4~~6. Processing steps for automatically generating the S1 or RCM synthetic aperture radar (SAR) image stack selection.

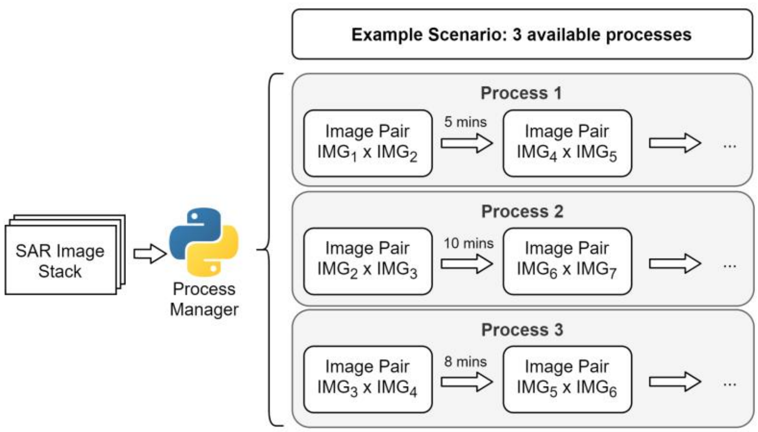

~~**Figure 5.**~~ **Figure 7. Illustration of the horizontal scalability approach used to process S1 or RCM image stacks.**

The final step ~~involved~~ involves combining the results of the automatic S1 and RCM SIM tracking process into defined spatial and temporal resolution grids to be used for analysis and mapping (Fig. ~~3~~2). Combining the SIM output from S1 with RCM (i.e., S1+RCM) ~~facilitated~~ facilitates the ability to improve the spatial coverage ~~and~~ because of S1+RCM image density ~~of SAR generated SIM~~ across the Arctic (Fig 3.). ~~For example, the spatial distribution of SAR image density per week in 2020 for S1, RCM and S1+RCM is shown in Fig. 6. S1 had a denser coverage compared to RCM for the majority of the Arctic regions and especially the Central Arctic and Greenland Sea. However, RCM coverage was more widely spread across the Arctic compared to S1 and extended into to the Bering Sea, Labrador Sea, and over the North Pole thus filling a gap typically associated with the majority of satellite sensors. An example of the ability of RCM to almost completely cover the~~

~~North Pole on a single day is shown in Fig. 7~~. In addition, S1+RCM image density increases with latitude (Fig. ~~6~~3) indicating that more consistent coverage of the ice pack will be possible during the melt season which is beneficial considering this is when automated SIM tracking algorithms have more difficulty. ~~Clearly, SAR image density from S1+RCM from March to December 2020 was significant (Fig. 6) with almost complete coverage every 3-days.~~ Two datasets are routinely produced: 7-day 25 km and 3-day (rolling) 6.25 km. The former is to represent a spatial complete picture of SIM generated from SAR and the latter to provide a more high resolution dataset that can benefit applications requiring higher spatiotemporal resolution. ~~However, despite the high image density coverage from S1+RCM, more consistent pan-Arctic SIM coverage can be achieved over 7-days because there are more image overlaps during a longer time span. As a result, a 25 km spatial resolution with a temporal resolution of 7-day was selected to provide the most consistent S1+RCM SIM coverage across the pan-Arctic domain.~~ It should be noted that based on S1+RCM image density shown in Fig. ~~6~~ 3 regional S1+RCM SIM products at higher spatial and temporal resolution are certainly achievable ~~given the image density S1+RCM~~and ECCC-ASITS can be modified to produce SIM to very localized studies (e.g. Moore et al., 2021a Moore et al., 2021b).~~,~~ ~~and as a result we also briefly demonstrate this capability in the results section.~~

For each grid cell, at least 5 individually tracked SIM vectors had to be within a distance of 3 times grid cell resolution cell centroid. Considering the SIM vectors are determined at a spatial resolution of 200 m and gridding takes place at 25 km and 6.25 km, numerous vectors are within the grid cell. Only SIM vectors estimated from image pairs with a time separation of greater than 12 hrs were considered. We selected a 12 hrs cut-off because below 12 hrs the SIM resulted in less representative (usually higher speeds) with respect to the averaged product value (over 3 or 7 days). This was the primary observation from previous studies constructing a very high temporal resolution time series (e.g. Howell and Brady, 2019; Moore et al., 2021a). Use of ice displacement vectors derived from images with lower time separation (< 12 hrs) would lead to less representative (more uncertain) average ice speeds in 3 or 7 days average SIM products. In addition, SIM vectors with speeds greater than 75 km/day where filtered out because based on manual inspection of automatically detected SIM vectors there are sometimes unrealistic anomalous SIM vectors with speeds greater than 75 km/day. ~~In order to control for SIM speed heterogeneity within a 25 km grid cell, the median SIM was used to represent the ice speed for each grid cell.~~ For each grid cell, a series of descriptive statistics ~~were~~ are calculated that include~~d~~ the number of S1~~and~~ +RCM SIM vectors, the ~~median~~ mean ~~SIM~~u and v, ~~the standard deviation of SIM~~, ~~and~~ the mean cross-correlation coefficient, and an estimate of speed uncertainty for dry and wet sea conditions (see Section 5). Even after removing anomalously large SIM speeds, the automatic SIM tracking algorithm sometimes detected obviously erroneous SIM vectors far from the marginal ice zone and/or near the coast in sufficient quantity (i.e. 5+) to meet the grid cell criteria. These grid cells were subsequently filtered out using a threshold distance of 150 km from the marginal ice zone (i.e., ice concentration of at least 18%) using the weekly National Ice Center ice charts.

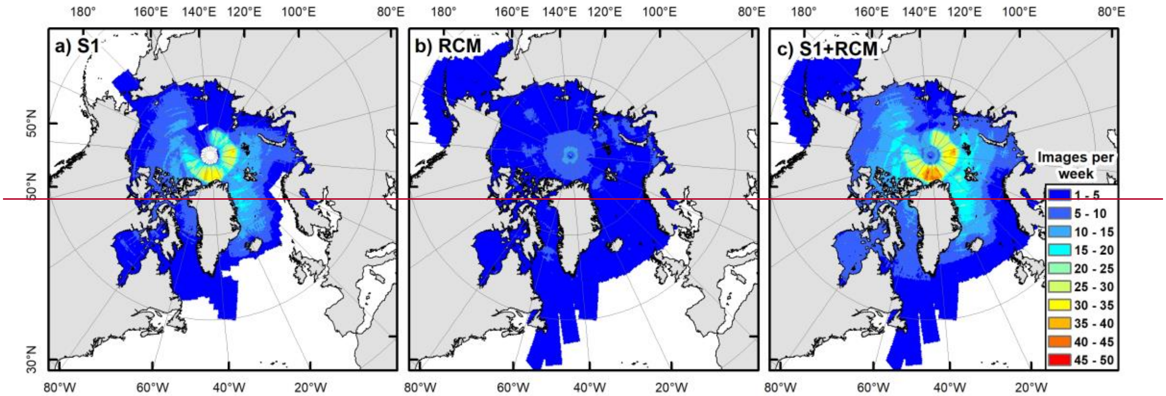

~~Figure 6. Image density per week for a) S1, b) RCM, and c) S1+RCM.~~

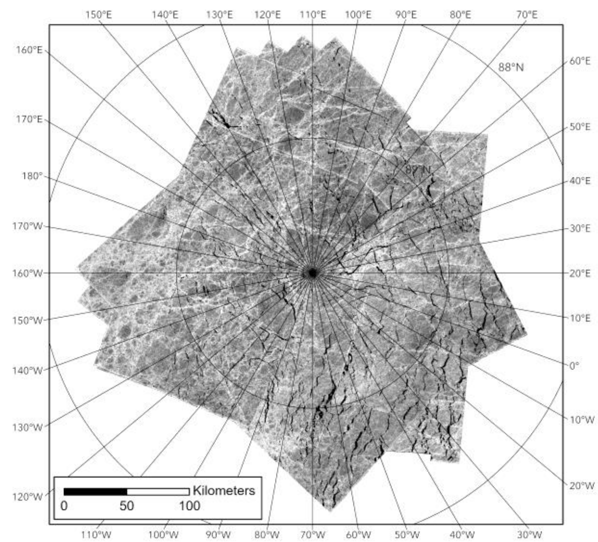

~~Figure 7.~~ Figure 4. **RCM image coverage over the North Pole on September 15, 2020. RADARSAT Constellation Mission Imagery © Government of Canada 2020. RADARSAT is an official mark of the Canadian Space Agency.**

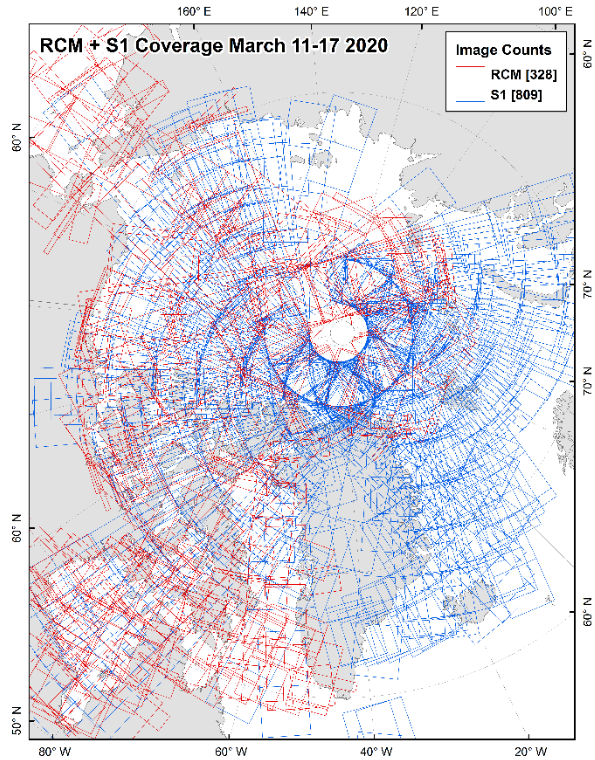

Figure 5. Spatial distribution of S1 and RCM SAR images from March 11-17, 2020.

~~3.3 Quantifying vector quality and uncertainty~~

~~The automated SIM tracking algorithm utilized in this study has undergone extensive validation against buoy positions and has an uncertainty of 0.43 km derived for SAR image pairs separated by 1-3 days (Komarov and Barber, 2014). Moreover, SIM output from the tracking algorithm has been found to be in good agreement with other tracking algorithms that includes the RADARSAT Geophysical Processor (e.g. Kwok, 2006; Agnew et al., 2008; Howell et al., 2013). However, considering the application of the tracking algorithm in this study represents considerably larger spatial and temporal domains it is important to assess the quality and uncertainty of the S1+RCM SIM vectors. To provide a quality assessment of the S1+RCM SIM vectors for each grid cell, the cross-correlation coefficient for all S1+RCM vectors in each grid cell were averaged. However, in order estimate the SIM uncertainty of all the S1+RCM vectors in each grid cell, a more structured approach was adopted.~~

~~Let us consider a grid cell containing a set of~~ $\cancel{N}$ ~~sea ice velocity vectors~~ $\cancel{\vec{V}_i}$, ~~where~~ $\cancel{i = 1,2,\ldots,N}$. ~~Each vector has the following uncertainty associated with the SIM tracking algorithm deriving the ice motion vector from two consecutive images:~~

$$\cancel{\Delta V_i = \frac{s_\sigma}{\Delta t_i},} \qquad \cancel{(1)}$$

~~where, Δt_i is the time interval (in days) separating two SAR images used to derive the considered ice velocity vector $\vec{V}_i$. $s_\sigma = 0.43km$ is the uncertainty in sea ice displacement (not speed) reported by Komarov and Barber (2013). Note that s_σ was derived for the SAR images separated by a variable time interval (1-3 days), so it must be divided by Δt_i to come up with the ice velocity uncertainty. The average velocity value assigned to the considered grid cell is the following:~~

$$\vec{V}_i = \frac{1}{N}\sum_{i=1}^{N}\vec{V}_i \, . \qquad (2)$$

~~The SIM uncertainty of each grid cell, σ_{SIM} can be estimated as follows:~~

$$\sigma_{SIM} = \frac{\sigma_0}{\sqrt{1-\alpha^2}}, \qquad (3)$$

~~where, σ_0 is the base uncertainty given as follows:~~

$$\sigma_0 = \left\{\frac{1}{N}\sum_{i=1}^{N}\Delta V_i^2\right\}^{0.5}, \qquad (4)$$

~~and α is the uncertainty score (varying from 0 to 1) associated with the methodology used to aggregate N individual ice motion vectors derived from pairs of images into the SIM product:~~

$$\alpha = \{\frac{1}{3}[(c_{max} - \bar{c})^2 + (1-\tau)^2 + (1-n)^2]\}^{0.5} \qquad (5)$$

~~where, $\bar{c}$ is the average cross-correlation coefficient within each grid cell, c_{max} is the maximum cross-correlation coefficient within each grid cell. $\tau = \frac{t_{SAR}}{T}$ is the fraction of time when SAR imagery are available. Here, t_{SAR} represents the time interval when SAR data were available over the entire time interval considered (T). $n = \frac{N}{N_{max}}$ is the relative number of ice motion vectors used to create the aggregated mean ice velocity vector $\vec{V}$. Here, N is the number of ice motion vectors within the cell, and N_{max} is the maximum possible number of the ice motion vectors for a grid cell.~~

~~4 Results and Discussion~~

~~4.1 S1+RCM sea ice motion~~

~~4.1.1 Pan-Arctic~~

~~Table 2 shows the number of SIM vectors detected for the pan-Arctic and each sub-region (Fig. 1) based on over 60,000+ S1 and RCM images available over the period of March to December 2020. On average, there were 4,555,186 SIM vectors detected each week for 2020. The majority (~60%) were located in the Central Arctic sub-region that contains the perennial Arctic sea ice pack and also has a very high weekly S1+RCM image density (Fig. 6).~~

~~Fig. 8 illustrates the time series of 7-day ice speed from S1+RCM averaged over the entire pan-Arctic domain from March to December, 2020. The ice speed seasonal cycle as detected by S1+RCM was clear with ice speed decreasing during the melt season and increasing into the fall and winter.~~

~~An example of the spatial distribution of S1+RCM SIM on March 11-17, 2020 and December 16-22, 2020 is shown in Fig. 9. Notable features for March include the Transpolar Drift, counter-clockwise SIM characteristic of a Beaufort Gyre reversal, and landfast (no ice motion) ice conditions within the majority of the CAA. The most notable feature for December~~

~~was the clockwise SIM characteristic of the Beaufort Gyre. For the March 11-17 example, the spatial coverage was extensive with the exception of a gap within the Laptev Sea which is to be expected based the weekly image density (Fig.6). For the December 16-22 example, the spatial coverage was also extensive and included in the Laptev Sea. Overall, the high density image coverage achieved with S1+RCM was able to provide weekly SAR derived estimates of SIM across the Arctic for 2020.~~

~~Table 2. Average number of S1+RCM sea ice motion vectors detected per week for the Arctic from over the period of March to December 2020.~~

~~**Region**~~	~~**Number of Vectors**~~
~~Baffin Bay/Labrador Sea~~	~~84,163~~
~~Barents Sea~~	~~68,522~~
~~Beaufort Sea~~	~~534,168~~
~~Bering Sea~~	~~11,169~~
~~Canadian Arctic Archipelago~~	~~79,316~~
~~Chukchi Sea~~	~~369,844~~
~~East Siberian Sea~~	~~346,031~~
~~Greenland Sea~~	~~136,171~~
~~Central Arctic~~	~~2,725,437~~
~~Hudson Bay~~	~~89,624~~
~~Kara Sea~~	~~104,453~~
~~Laptev Sea~~	~~49,771~~
~~Pan-Arctic~~	~~4,555,186~~

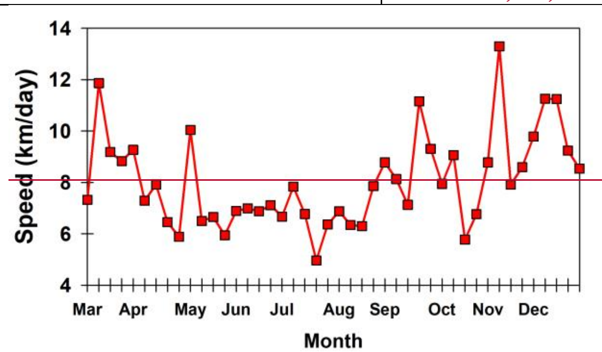

~~Figure 8. The time series of 7-day ice speed from S1+RCM averaged over the entire pan-Arctic domain from March to December, 2020. Only ice speeds > 0 were used to calculate the averages (i.e., no zero SIM data were used).~~

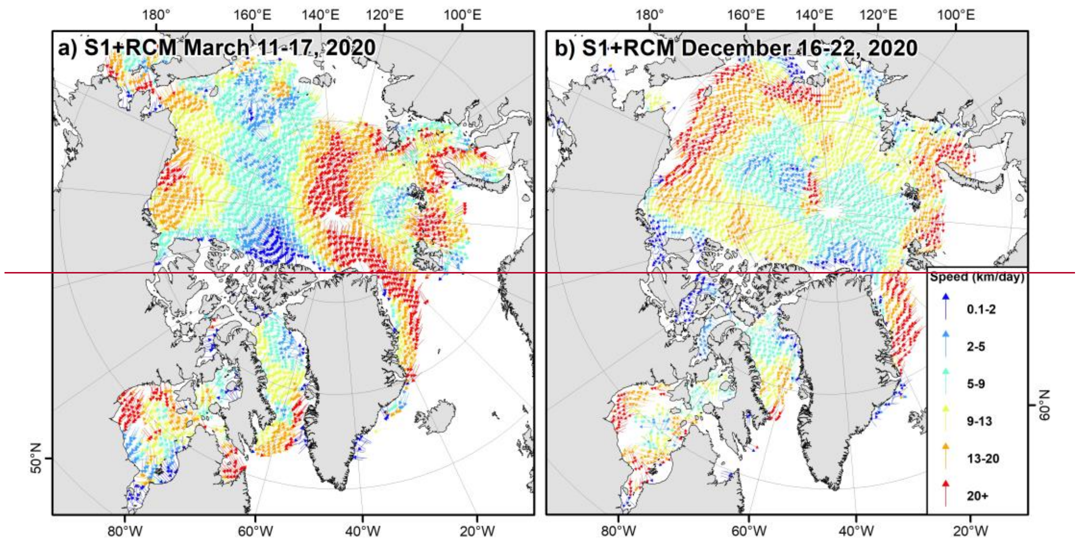

~~**Figure 9. The spatial distribution of S1+RCM sea ice motion on a) March 11-17, 2020 and b) December 16-22, 2020. Note that the white areas in the figure indicate either zero ice motion for the landfast ice or no ice motion information extracted (because of no SAR data, no ice, or no stable ice features).**~~

~~4.1.2 Canadian Arctic Archipelago (CAA)~~

~~Although not the primary focus of this study, Fig. 6 underscores that in addition to pan-Arctic S1+RCM SIM products, high spatial and temporal resolution regional S1+RCM products are certainly achievable for 2020. To that end, we generated 12.5 km, 7-day S1+RCM SIM for the CAA from March to December, 2020. The CAA is a region where SIM is not typically well resolved from coarser resolution satellites because of its narrow channels and inlets which makes automated SIM tracking difficult, especially during the melt season. Resolving SIM within the CAA (and during the melt season) was achieved because S1+RCM SIM vectors are initially derived at a spatial resolution of 200 m, therefore, alleviating the main limitation of coarser resolution sensors. The annual cycle of ice speed time series shown in Fig. 10 is representative of the CAA being mostly landfast from November to July as ice speed is typically slow and confined to the periphery regions (Agnew et al., 2008). The spike in June was associated with an ice fracture in eastern periphery of the CAA (not shown). An example of the S1+RCM SIM spatial distribution from August 12-18 at 12.5 km is shown in Fig. 11 and illustrates the considerable spatial variability of SIM within the CAA.~~

~~Given the considerable weekly image density available from S1 and RCM, further enhances in spatial and temporal resolution for more local scale SIM studies are also possible (e.g. Moore et al., 2021). Although the focus of this study is primarily large-scale SIM the latter point is important to demonstrate. Figure 12 illustrates and example of how SIM can be resolved from resolutions of 6.25 km, 12.5 km, and 25 km for a 3-day temporal resolution within the middle of CAA. The level of detail that can be resolved at even 6.25 km is striking and even further increases are possible given the original 200 m spatial resolution.~~

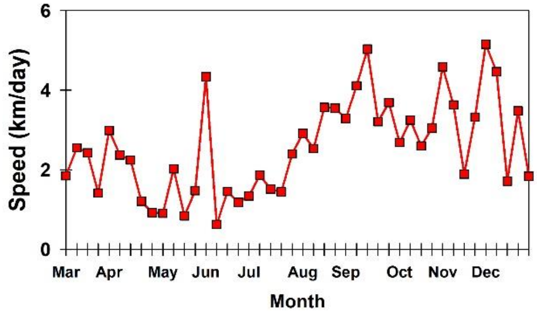

~~Figure 10. The time series of 7-day ice speed from S1+RCM averaged over the Canadian Arctic Archipelago from March to December, 2020. Only ice speeds > 0 were used to calculate the averages (i.e., no zero SIM data were used).~~

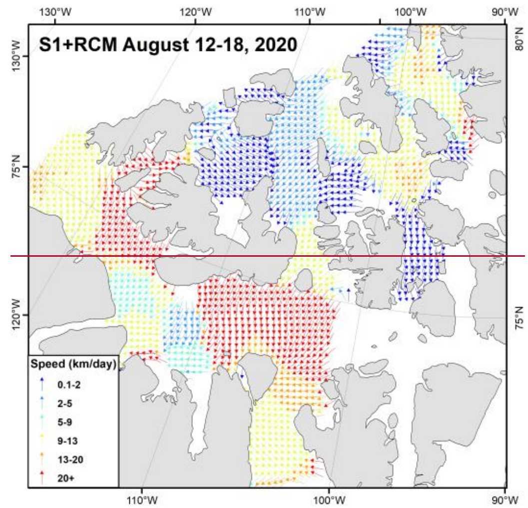

~~Figure 11. The spatial distribution of S1+RCM sea ice motion on August 12-18, 2020 in the Canadian Arctic Archipelago. Note that the white areas in the figure indicate either zero ice motion for the landfast ice or no ice motion information extracted (because of no SAR data, no ice, or no stable ice features).~~

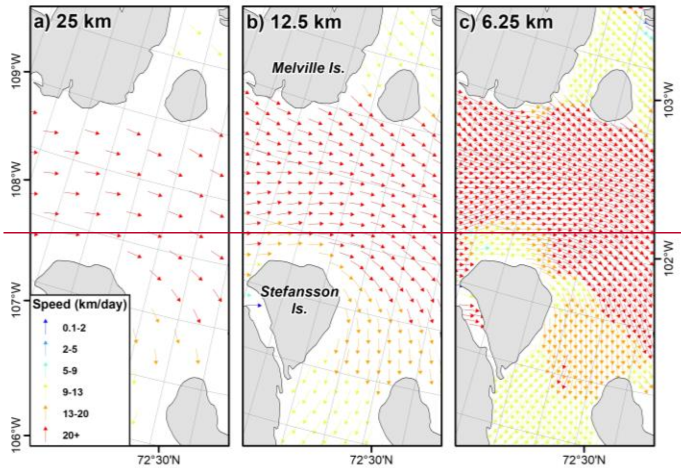

~~**Figure 12. The spatial distribution of S1+RCM sea ice motion on August 12-18, 2020 in the middle of the Canadian Arctic Archipelago at spatial resolutions of a) 25 km, b) 12.5 km, and c) 6.25 km.**~~

~~4.2 Spatiotemporal variability of sea ice motion vector quality and uncertainty~~

~~Figure 13 shows the time series of the S1+RCM weekly average of the cross-correlation coefficients and σ_{SIM} across the pan-Arctic. Note that for automated SIM tracking algorithm used in this study, the cross-correlation coefficients are calculated for the second order derivatives (Laplacians) of the images, and not the original images; therefore, the cross-correlation coefficients may appear lower than reported in the literature by other studies. Both the cross-correlation coefficient and σ_{SIM} exhibited the expected variability associated with the seasonal cycle of sea ice and remained relatively high and stable during the dry winter conditions, decreased during the melt season and then returned to stability following the melt season (Fig. 13). σ_{SIM} was initially high in early-March because of lower amounts RCM imagery when it first became operational (Fig. 13). As found in previous studies, higher σ_{SIM} and lower quality vectors are more apparent during the shoulder seasons (i.e. melt-freeze transitions) as a result of water on the surface of the ice and low ice concentration making automated feature tracking more difficult (e.g., Agnew et al., 2008; Lavergne et al., 2010). Moreover, there are also fewer vectors detected during the shoulder seasons compared to dry winter conditions which contributes to higher σ_{SIM}.~~

~~Figure 14 illustrates the σ_{SIM} spatially for selected weekly periods during the 2020 annual cycle. For all cases, σ_{SIM} values are typically found in the central Arctic and gradual increases outwards (Fig. 14). The observed spatial variability of σ_{SIM} is in part related to weekly SAR image density that decreases away from the central Arctic because they are primarily only covered by RCM (Fig.6). For example, higher σ_{SIM} was observed in the periphery regions of the Beaufort Sea, Hudson Bay, and the Bering Sea during March 11-17 (Fig. 14a) and in Lapev Sea for December 16-22 (Fig. 14d). σ_{SIM} was lower during the summer months but the weekly image density of S1+RCM (Fig. 6), provided considerably more images over the marginal ice zones during the melt season. As a result, there are more image data to better resolve challenging ice conditions during the shoulder as shown from August 11-17 (Fig. 14b) and September 30-October 7 (Fig. 14c).~~

~~Figure 15 summarizes σ_{SIM} and the cross-correlation coefficient using box-plots for the each Arctic sub-region from March to December 2020. The interquartile range for most sub-regions were between 0.35-0.45 for the cross-correlation coefficient (Fig. 15a) and between 0.4-0.6 km/day for σ_{SIM} (Fig.15b). The largest σ_{SIM} was found in Bering Sea and the lowest in the Central Arctic (Fig. 15b). Lower cross-correlation coefficients were more apparent for regions that contain a significant portion marginal ice zone in 2020 (e.g. East Siberian Sea, Chukchi Sea, and Greenland Sea). Based on Fig.15, the association between higher (lower) σ_{SIM} and lower (higher) cross-correlation coefficients was not always apparent at the sub-region scale because of the variability of each regions sea ice physical characteristics over the annual cycle. Depending on how ice conditions evolve during the melt season, the distribution of regions with low ice concentrations may vary accordingly. Sub-region σ_{SIM} may also change regionally in subsequent years depending if the weekly pan-Arctic S1+RCM image density changes. To that end, the regional σ_{SIM} and cross-correlation coefficients values presented in Fig. 15 should be interpreted as initial or baseline values since we are only considering the year 2020.~~

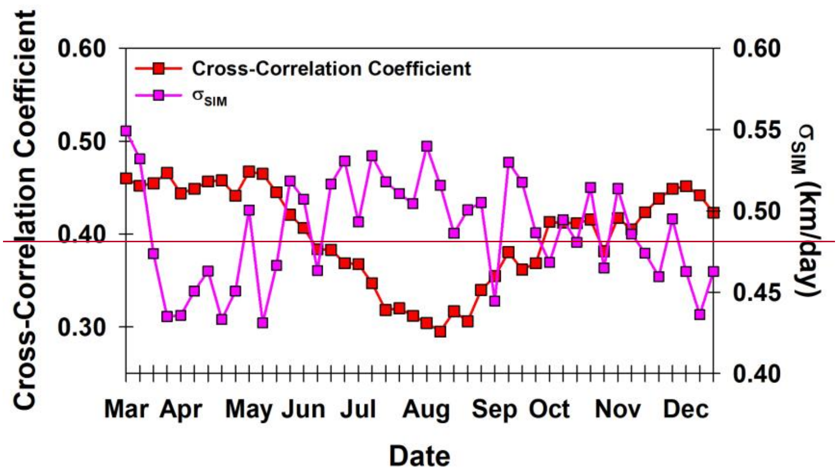

~~**Figure 13. Time series of the weekly average of sea ice motion cross-correlation coefficient and sea ice motion uncertainty (σ_{sim}) across the pan-Arctic from March to December, 2020.**~~

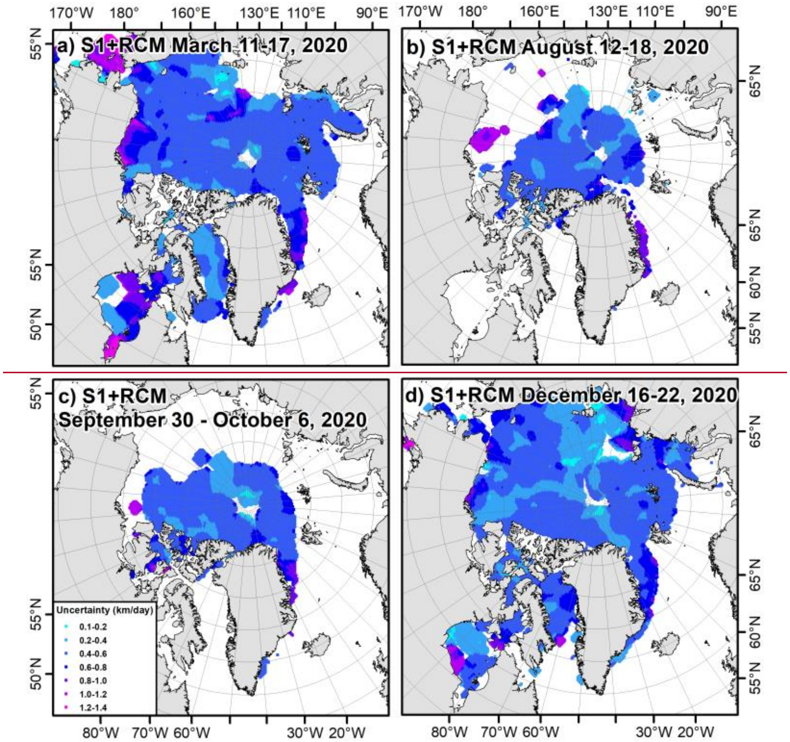

~~**Figure 14. Spatial distribution of S1+RCM sea ice motion uncertainty on a) March 11-17, 2020, b) August 12-18, c) September 30-October 6, and d) December 16-22, 2020. Note that the white areas in the figure indicate either zero ice motion for the landfast ice or no ice motion information extracted (because of no SAR data, no ice, or no stable ice features).**~~

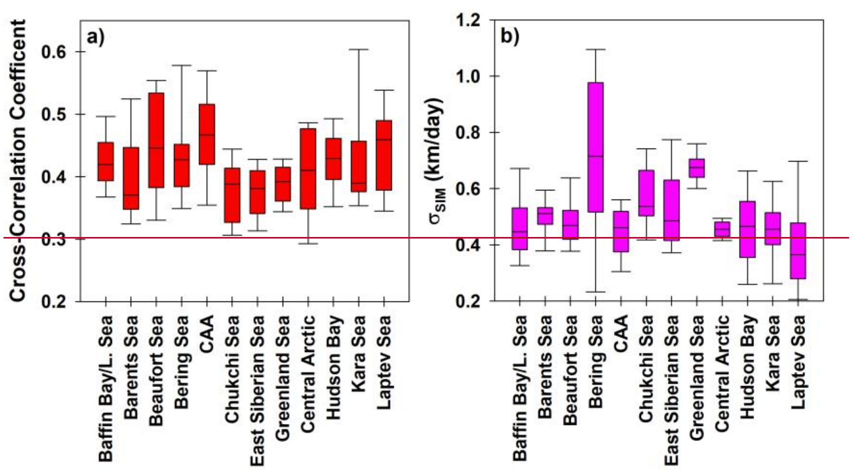

~~**Figure 15. Boxplots of the S1+RCM a) cross-correlation coefficient and b) sea ice motion uncertainty (σ_{sim}) for the Arctic sub-regions from March to December, 2020.**~~

4 Large-scale SIM from S1+RCM

Table 2 shows the average number S1+RCM SIM grid cells per month across the pan-Arctic for the 25 km 7-day and 6.25 km 3-day products from March 2020 to October 2021. Based on the resolvable S1+RCM grid cells, the 7-day 25 km spatiotemporal scale is able to provide the most complete picture of SIM across the pan-Arctic from SAR imagery alone. However, the higher temporal resolution of the 3-day SIM product captures more of the temporal variability. Examples of S1+RCM SIM over the pan-Arctic for selected weeks during winter months are shown in Fig. 8. Notable features include the Transpolar Drift (Fig. 8a; Fig. 8c), Beaufort Gyre (Fig. 8b), a Beaufort Gyre reversal (Fig. 8a), and minimal SIM because of landfast (no ice motion) ice conditions within the majority of the CAA (Fig. 8). Some spatial gaps are present in certain weeks, particularly in the Laptev Sea (Fig. 8) and these gaps, in addition to others are because of the spatial variability in weekly image density of S1+RCM (Fig. 3). Despite some spatial gaps, an average 16,000+ grid cells containing S1+RCM SIM estimates per week during the winter months were resolved for 2020 and 2021 (Table 2).

Resolving SIM during the melt season, even with high spatial resolution SAR imagery, is more challenging than dry winter conditions because automated feature tracking is more difficult when the ice concentration is low or water is on the ice surface (e.g. Agnew et al., 2008; Lavergne et al., 2010). The average number of grid cells containing S1+RCM SIM during the summer months decreased by ~40% compared to the winter period (Table 2) but this decrease is also from summer melt. Examples of the spatial distribution of 25 km 7-day S1+RCM SIM for selected weeks summer months are shown in Fig. 9 and indeed the spatial coverage from S1+RCM is still considerable during the summer months.

Table 2. Average number S1+RCM SIM grid cells per month across the pan-Arctic that are resolved at for the 25 km 7-day and 6.25 km 3-day products from March 2020 to October 2021

Month	7-day 25 km S1+RCM SIM Grid cells		3-day 6.25 km S1+RCM SIM Grid cells	
	2020	2021	2020	2021
January		16,373		106,315
February		16,803		75,946
March	15,500	17,050	107,901	116,919
April	15,548	16,758	99,735	118,624
May	14,387	15,449	80,812	91,334
June	13,316	13,901	63,519	66,678
July	9,466	10,436	35,621	45,449
August	6,220	7,537	20,934	32,940
September	5,683	7,400	34,989	47,386
October	7,864	10,242	54,597	69,052
November	11,023		72,117	
December	15,189		99,626	

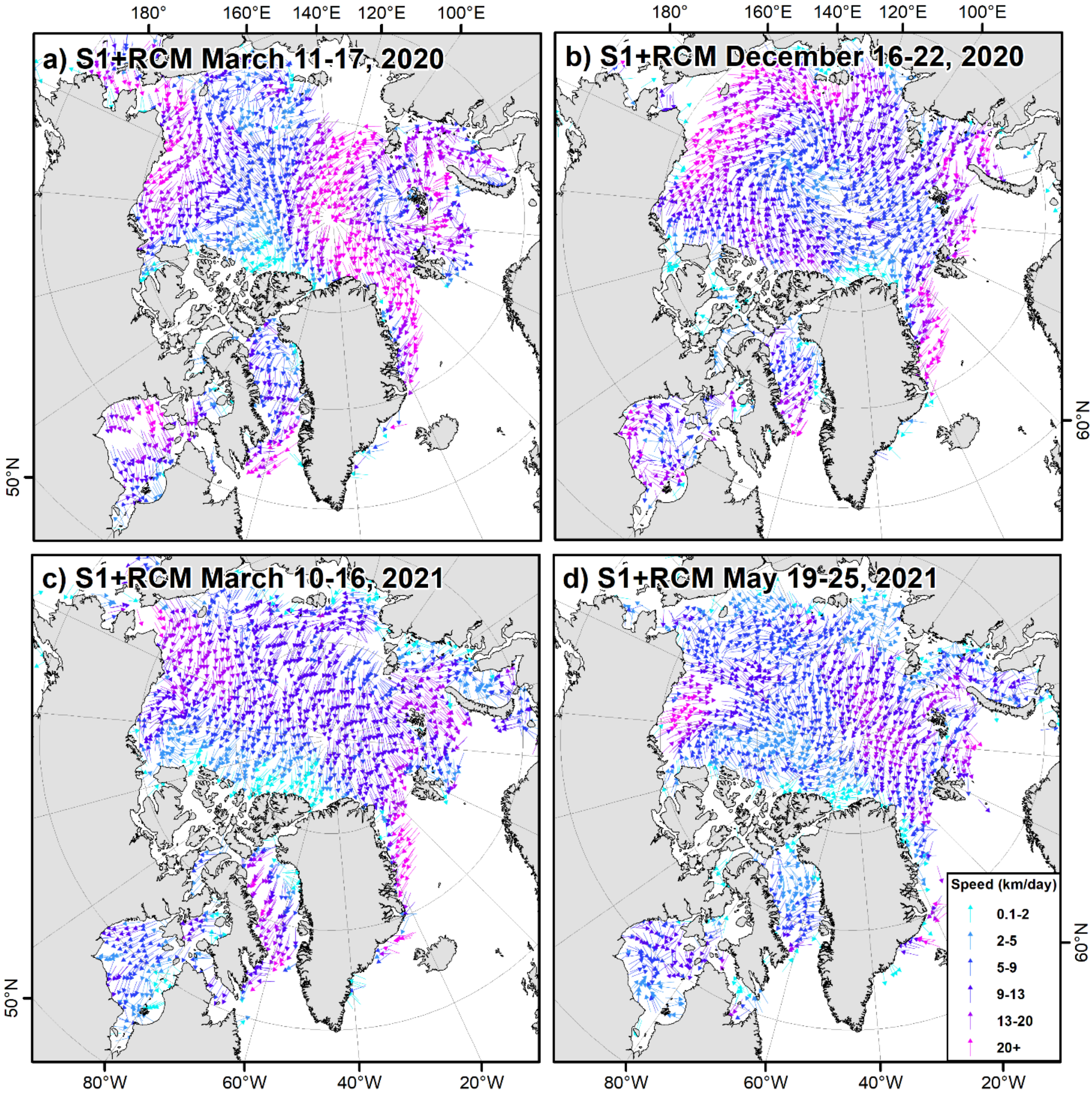

Figure 8. The spatial distribution of 25 km 7-day S1+RCM sea ice motion on a) March 11-17, 2020, b) December 16-22, 2020, c) March 10-16, 2021, and d) May 19-25, 2021. Note that the white areas in the figure indicate either zero ice motion for the landfast ice or no ice motion information extracted (because of no SAR data, no ice, or no stable ice features).

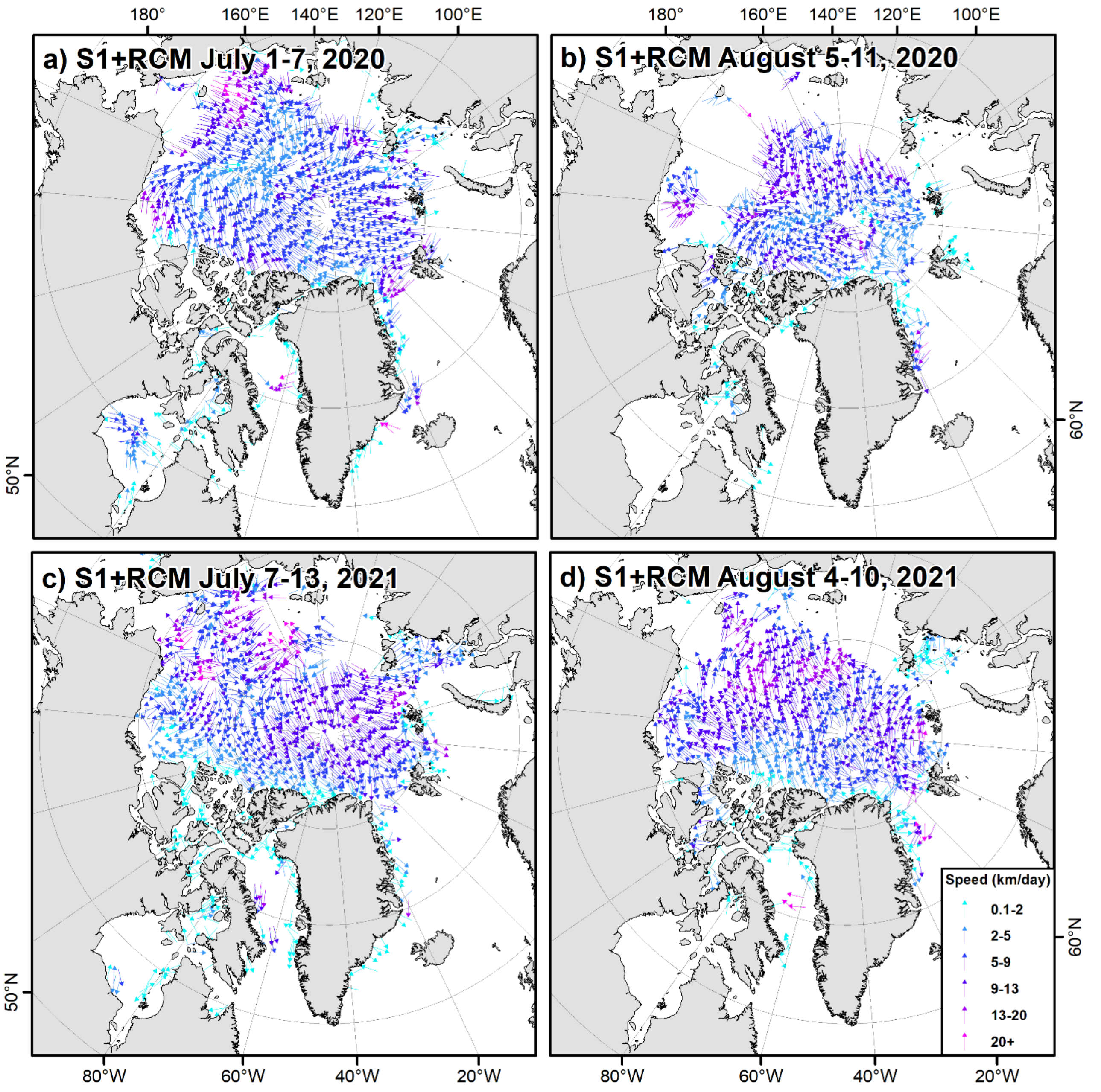
a) S1+RCM July 1-7, 2020
b) S1+RCM August 5-11, 2020
c) S1+RCM July 7-13, 2021
d) S1+RCM August 4-10, 2021
180°
160°E
140°E
120°E
100°E
50°N
60°N
80°W
60°W
40°W
20°W
Speed (km/day)
0.1-2
2-5
5-9
9-13
13-20
20+

Figure 9. The spatial distribution of 25 km 7-day S1+RCM sea ice motion on a) July 1-7, 2020, b) December 5-11, 2020, c) July 7-13, 2021, and d) August 4-10, 2021. Note that the white areas in the figure indicate either zero ice motion for the landfast ice or no ice motion information extracted (because of no SAR data, no ice, or no stable ice features).

The spatial distribution of 6.25 km 3-day pan-Arctic S1+RCM SIM for selected periods during the winter and summer are is shown in Fig. 10 and Fig. 11, respectively. Although considerably more grid cells are contained S1+RCM SIM (Table 2), there are more spatial gaps across the pan-Arctic using higher spatiotemporal resolution especially, during the summer months. Despite this, there are still many regions across the Arctic where high spatial and temporal SIM can be resolved using S1+RCM. The insets of both Fig. 10 and Fig. 11 illustrate the level of SIM spatial detail captured at 6.25 km.

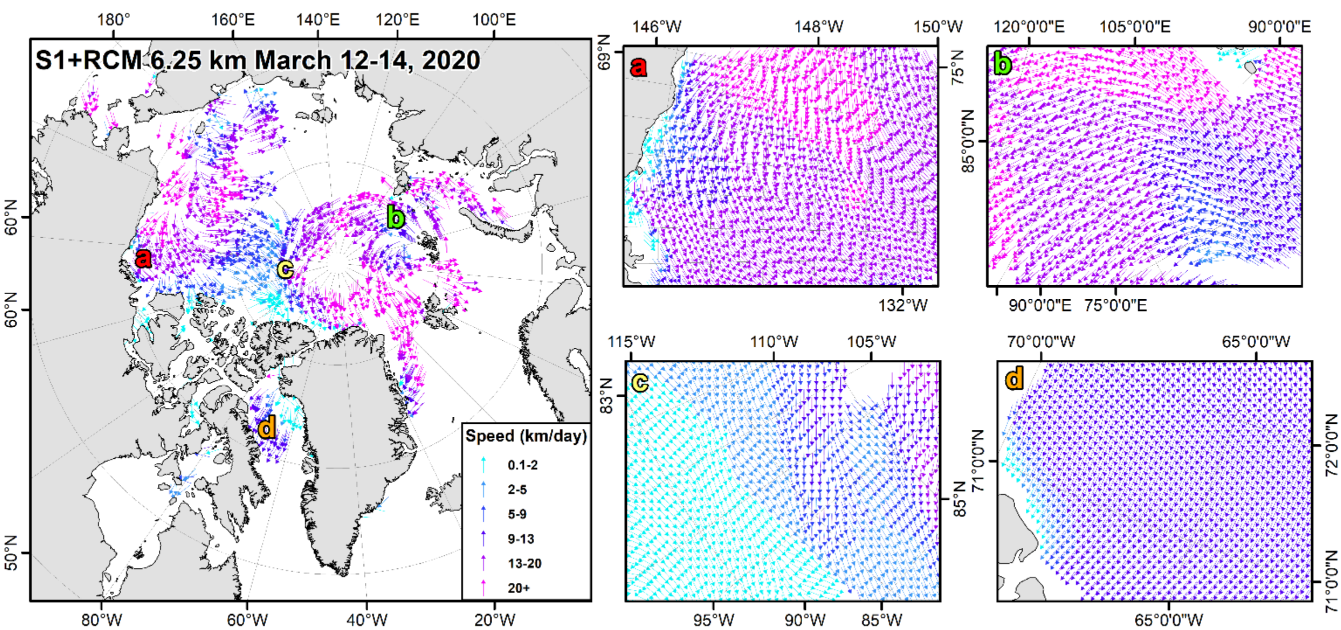

Figure 10. The spatial distribution of 6.25 km 3-day S1+RCM sea ice motion on March 12-14, 2020. The letters correspond to zoomed in regions on the map. Note that the white areas in the figure indicate either zero ice motion for the landfast ice or no ice motion information extracted (because of no SAR data, no ice, or no stable ice features).

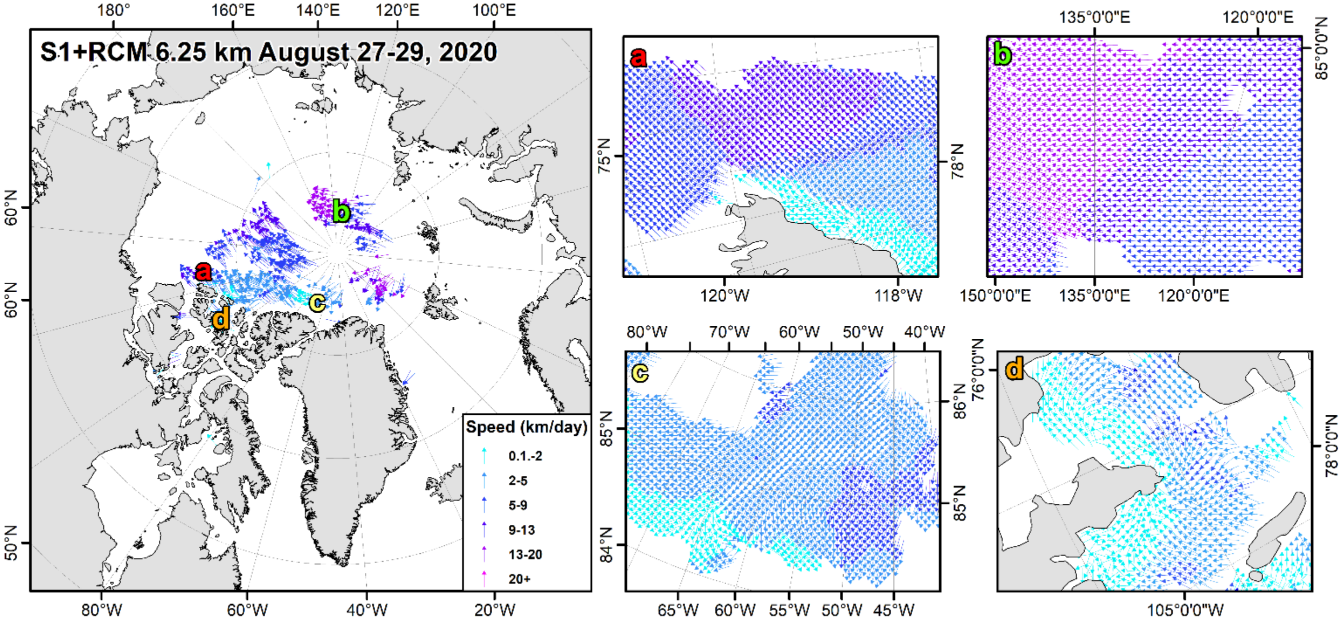

Figure 11. The spatial distribution of 6.25 km 3-day S1+RCM sea ice motion on August 27-29, 2020. The letters correspond to zoomed in regions on the map. Note that the white areas in the figure indicate either zero ice motion for the landfast ice or no ice motion information extracted (because of no SAR data, no ice, or no stable ice features).

In both S1+RCM SIM products, SIM is resolved within the CAA, and Fig 12. provides a more detailed look at summer SIM within the CAA. Indeed SIM in this region is very spatially heterogeneous as pointed out by Melling (2002). Estimating SIM within the CAA is challenging for coarse resolution satellites because its narrow channels and inlets that make automated feature tracking difficult, especially during the melt season (Agnew et al., 2008) and this is a major gap with existing SIM products. Information on SIM within the CAA is important given it contains the Northwest Passage and has experienced increased in shipping activity (e.g. Dawson et al., 2018). Both large-scale S1+RCM SIM products generated by ECCC-ASIS provide valuable SIM information in this region not just for scientific analysis, but also for stakeholders operating in the CAA. Continued monitoring of SIM within the CAA is important as climate warming is expected make the region more navigable in the future (Mudryk et al., 2021).

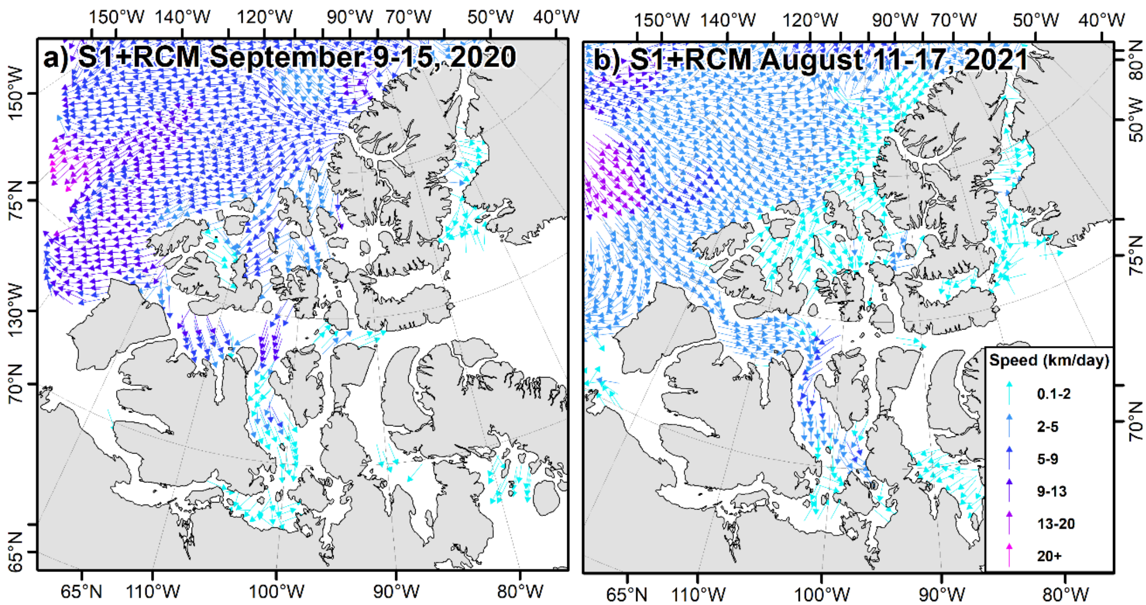

Figure 12. The spatial distribution of 25 km 7-day S1+RCM sea ice motion surrounding the Canadian Arctic Archipelago on a) September 9-15, 2020 and b) August 11-17, 2021. Note that the white areas in the figure indicate either zero ice motion for the landfast ice or no ice motion information extracted (because of no SAR data, no ice, or no stable ice features).

5 S1+RCM SIM validation and assessing uncertainty

ECCC's automated SIM tracking algorithm has previously undergone validation against buoy positions and has an uncertainty of 0.43 km derived for RADARSAT-2 SAR image pairs separated by 1-3 days (Komarov and Barber, 2014). Moreover, SIM output from the tracking algorithm has been found to be in good agreement with other tracking algorithms that includes the RADARSAT Geophysical Processor (e.g. Kwok, 2006; Agnew et al., 2008; Howell et al., 2013). However, considering the application of the tracking algorithm in this study represents considerably larger spatial and temporal domains, together with new satellites sensors (i.e. S1 and RCM), it is important to reassess the quality and uncertainty of the resulting S1+RCM SIM vectors.

To provide a quality assessment of the S1+RCM SIM vectors for each grid cell the cross-correlation coefficient for all S1+RCM vectors in each grid cell were averaged. Fig. 13 summaries the monthly cross-correlation coefficients of 6.25 km 3-day S1+RCM SIM using boxplots. Note that for the ECCC automated SIM tracking algorithm, the cross-correlation coefficients are calculated for the second order derivatives (Laplacians) of the images, and not the original images; therefore, the cross-correlation coefficients may appear lower than reported in the literature by other studies. The cross-correlation coefficient exhibited the expected variability associated with the seasonal cycle of sea ice and remained relatively high and stable during the dry winter conditions (~0.45), decreased during the melt season (~0.33) and then returned to stability following the melt season (~0.45). As found in previous studies, lower quality vectors are more apparent during the shoulder seasons (i.e. melt-freeze transitions) (e.g., Agnew et al., 2008; Lavergne et al., 2010; Lavergne et al., 2021).

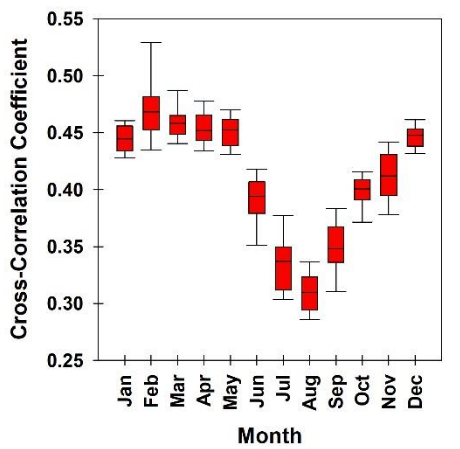

Figure 13. Boxplots of the monthly cross-correlation coefficient based on S1+RCM SIM from March 2020 to October 2021

In order to estimate the SIM uncertainty from the ECCC's automated SIM tracking algorithm for S1 and RCM SAR images, we compared SIM displacement vectors from S1 and RCM to buoy positions from the IABP during winter (April) and summer (August) time periods. For all S1 and RCM displacement vectors (derived from image pairs), the closest buoy trajectory was co-located to the start of each displacement vector position. The distance between the starting point of a given SAR ice motion tracking vector and the starting point of the corresponding buoy trajectory did not exceed 3 km. Fig 14. summarizes the results for dry winter conditions (April 2020 and 2021) and during the melt season (August 2020 and 2021). The ECCC automated SIM tracking algorithm performs very well during winter conditions with a root mean square error (RMSE) of 2.78 km and a mean difference (MD) of 0.40 km. The RMSE is higher than the value reported by Komarov and Barber (2014) likely because more image pairs over a larger geographical area were used in this comparison as well as the spatial resolution was lower. Performance slightly decreases during the summer with a lower number of vectors detected and an RMSE of 3.43 km.

Taking into consideration the difference between the winter and the summer we assign two uncertainties to the S1+RCM SIM products for dry and wet conditions as follows. Consider a grid cell containing a set of N sea ice velocity vectors $\vec{V}_i$, where $i = 1,2,\dots,N$. Ice speed for this each vector has the following uncertainty associated with the SIM tracking algorithm deriving the ice motion vector from two consecutive images:

$$\Delta V_i = \frac{s_0}{\Delta t_i}, \qquad (1)$$

where, Δt_i is the time interval (in days) separating two SAR images used to derive the considered ice velocity vector $\vec{V}_i$. In (1) s_o is the uncertainty in sea ice displacement (not speed) for dry ice conditions (2.78 km) or wet ice conditions (3.43 km). Note that s_o must be divided by Δt_i to come up with the ice velocity uncertainty. The average uncertainty for dry ($s_o = 2.78$ km) and wet ($s_o = 3.43$ km) ice conditions in each grid cell (N) is then determined using the following equation:

$$\sigma_{SIM} = \frac{1}{N}\sum_{i=1}^{N} \Delta V_i \qquad (2)$$

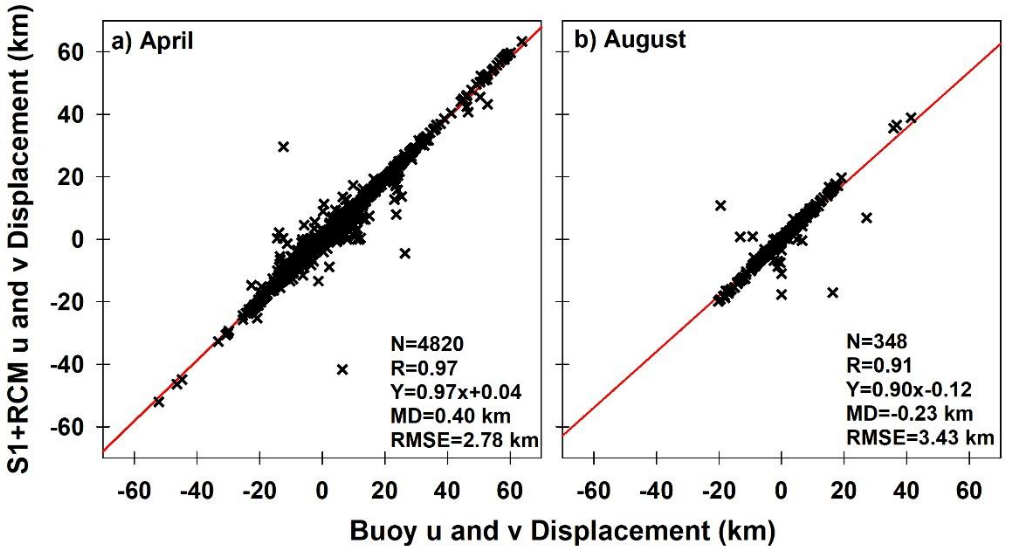

Figure 14. Comparison between ice motion vectors derived by the Komarov and Barber (2014) automated sea ice tracking algorithm from S1 and RCM SAR images and buoy data.

Fig. 15 shows an example of the spatial distribution of both dry and wet uncertainty estimates indicating higher uncertainty estimates for the latter. We acknowledge that it is difficult to quantify the impact of SAR image pair availability over 7-days together with automatic SIM vector detection under certain environmental conditions. The number of S1+RCM SIM vectors used in the grid cell generation can subsequently be used to account for this whereby, more confidence (less uncertainty) in SIM can be associated with a larger number of vectors. Moreover, S1+RCM image density increases with latitude (Fig. 3) indicating that more consistent coverage is available over the Central Arctic, which is also beneficial during the melt season when automated SIM tracking algorithms have more difficulty. However, SAR image pair coverage could be exceptional over the 7-day time window, yet environmental conditions (e.g., melt ponds, low ice concentration, marginal ice zone, etc.) could still make automatic SIM vector detection difficult resulting in a low number of SIM vectors in the grid cell. The problem of image coverage is less of a concern for the 3-day product given the average image separation is ~2-days. Given the difficultly in quantifying SAR image pair coverage on S1+RCM SIM uncertainty, we now compare S1+RCM SIM to existing products with different temporal resolutions. Such a comparison provides additional quantitative confidence metrics to assess the quality of the S1+RCM SIM estimates.

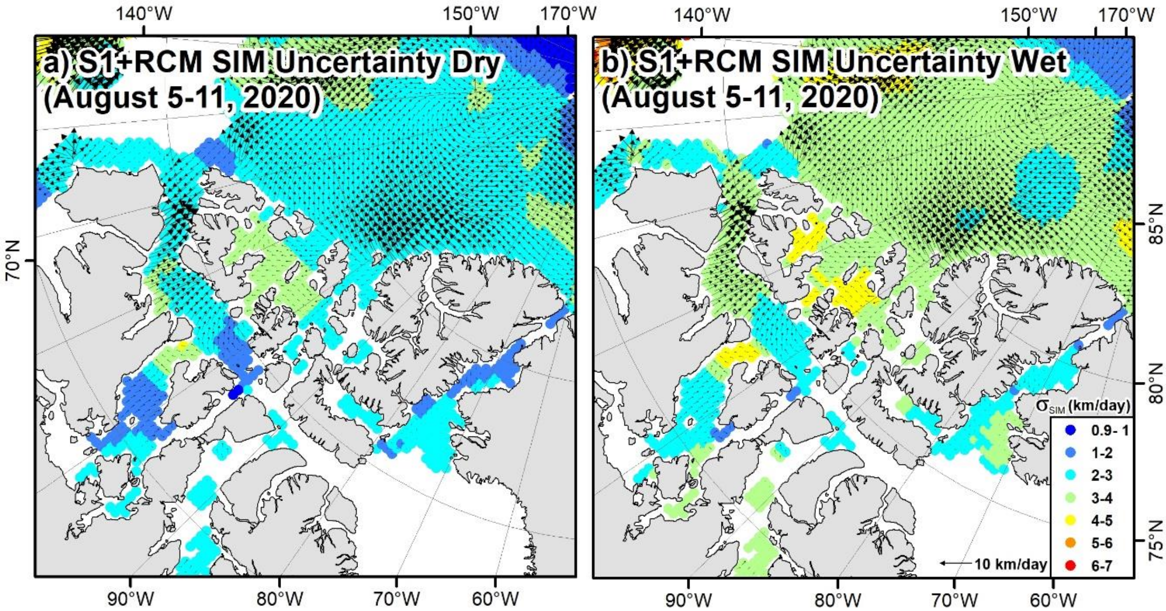

Figure 15. Spatial distribution of (a) dry and (b) wet S1+RCM SIM uncertainty for August 5-11, 2020

~~4.3~~6 SIM c~~C~~omparison of S1+RCM against NSIDC and OSI ~~-~~SAF

To facilitate a representative 1-to-1 grid cell comparison between S1+RCM SIM and both the NSIDC and OSI SAF SIM products, the spatial and temporal resolution of the S1+RCM were matched with the NSIDC and OSI SAF SIM products from March to December 2020. For OSI SAF, S1+RCM was generated with a 2-day at 62.5 km and for NSIDC, S1+RCM was generated with 7-day temporal resolution and 25 km spatial resolution. For each product's temporal resolution (i.e. 7-day for NSIDC and 2-day for OSI SAF), all the S1+RCM SIM vectors within each products grid cells (i.e. 25 km for NSIDC and 62.5 km for OSI-SAF) were averaged. This resulted in 455,905 grid cells for the S1+RCM and NSIDC comparison and 376,386 grid cells for the S1+RCM and OSI SAF comparison. More samples were available from NSIDC because of its higher spatial resolution.

Scatterplots of the u and v vectors components of SIM for S1+RCM versus NSIDC and OSI SAF are shown in Fig. 16 and 17, respectively. Both existing SIM products are in good agreement with S1+RCM with correlation coefficients for u and v of 0.75 and 0.78, respectively for the NSIDC and 0.84 and 0.85, respectively for OSI-SAF providing confidence in the SAR coverage for the 7-day and 3-day S1+RCM products. The RMSE is higher for the NSIDC (u=4.6 km/day and v=4.7 km/day) compared to OSI SAF (u=3.9 km/day and v=3.9 km/day), and we note the better agreement between S1+RCM and OSI SAF is likely because the temporal resolution more closely matches the average overlap between SAR images (i.e. ~2 days). However, the overall larger speed associated with S1+RCM is most likely the result of higher spatial resolution compared to lower resolution satellite data used in NSIDC and OSI SAF as faster speeds are more difficult to track at lower spatial resolution because of temporal decorrelation. Kwok et al. (1998) also noted this problem when comparing SIM from passive microwave with SAR and found it also applies to regions of low ice concentration. Figs. 16 and 17 also illustrate that users of either the NSIDC or OSI SAF SIM products are underestimating SIM.

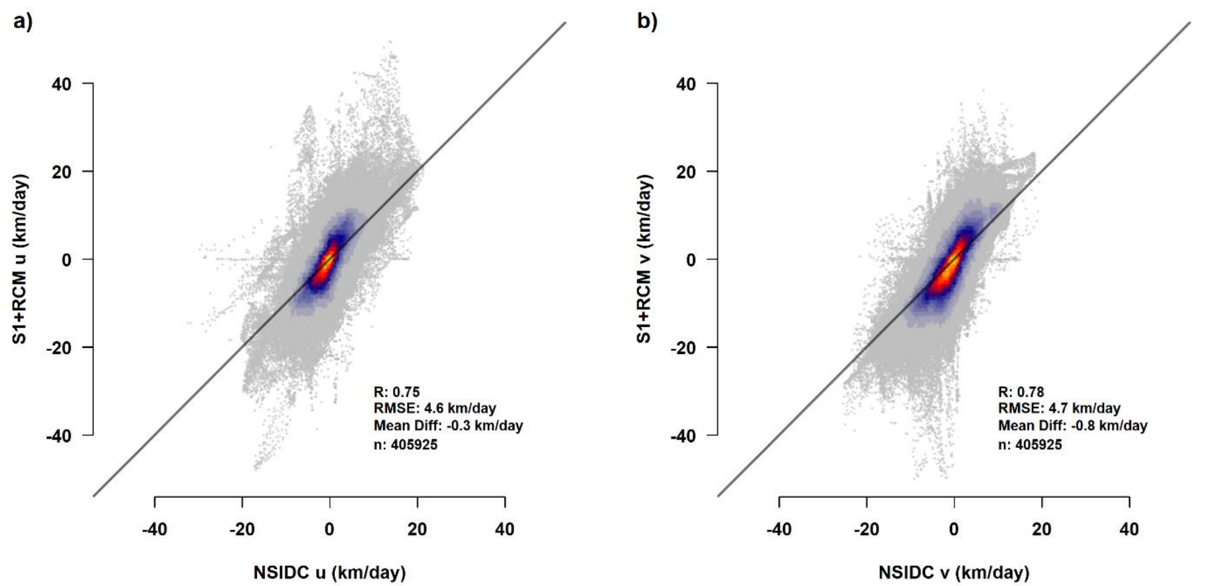

Figure 16. Scatterplots of S1+RCM sea ice motion versus National Snow and Ice Data Center (NSIDC) SIM for a) u and b) v vector components. Also shown is the number of samples (n), Pearson's correlation coefficient (R), root-mean square error (RMSE), and the mean difference (MD).

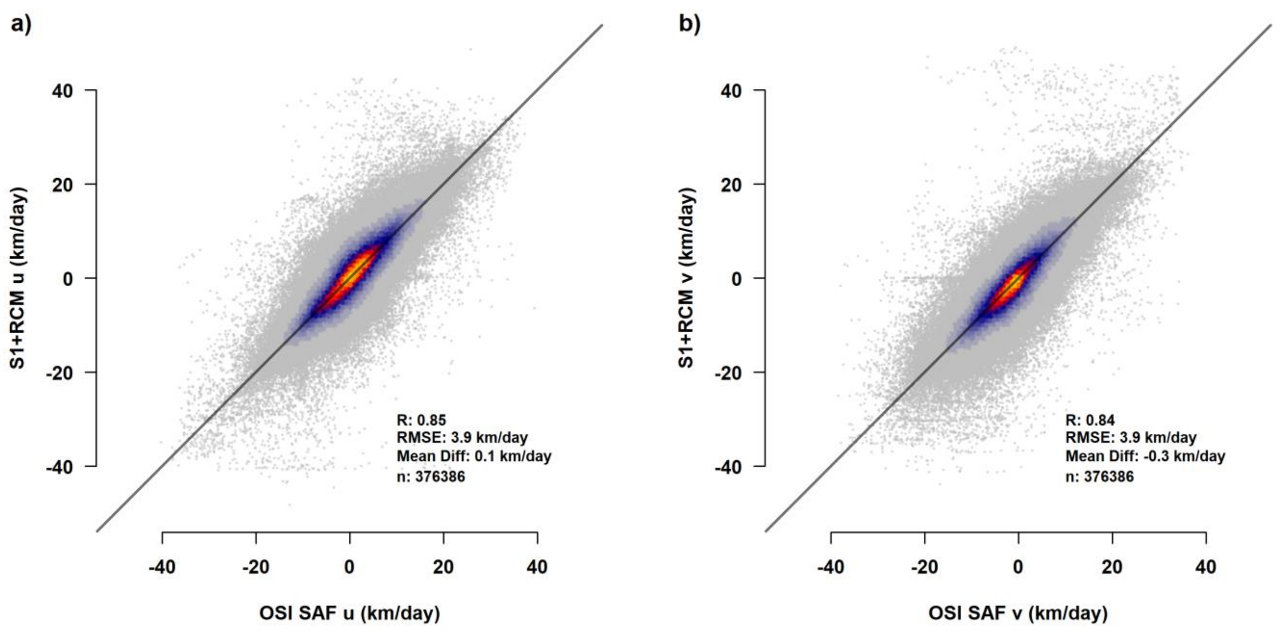

Figure 17. Scatterplots of S1+RCM sea ice motion versus Ocean and Sea Ice Satellite Application Facility (OSI SAF) SIM for a) u and b) v vector components. Also shown is the number of samples (n), Pearson's correlation coefficient (R), root-mean square error (RMSE), and the mean difference (MD).

~~Comparing our S1+RCM SIM results with existing NSIDC and OSI-SAF SIM products provides additional quantitative confidence metrics. In order to facilitate a representative 1-to-1 comparison between S1+RCM SIM and both the NSIDC and OSI-SAF SIM products, the spatial and temporal resolution of the S1+RCM were matched with the NSIDC and OSI-SAF SIM products for 2020. For OSI-SAF, S1+RCM was generated with a 2-day at 62.5 km and for NSIDC, S1+RCM was generated with 7-day temporal resolution and 25 km spatial resolution. For each product's temporal resolution (i.e. 7-day for NSIDC and 2-day for OSI-SAF), all the S1+RCM SIM vectors within each products grid cells (i.e. 25 km for NSIDC and 62.5 km for OSI-SAF) were averaged. The average of all the grid cells within each region across the Arctic (Fig.1) was then determined for all products. This resulted in 343 weekly averages for the S1+RCM and NSIDC comparison and 1957 2-day averages for the S1+RCM and OSI-SAF comparison. More samples were available from OSI-SAF because of the difference in temporal resolution of these two products (i.e., 2-day vs 7-day)~~

~~Scatterplots of S1+RCM versus NSIDC and OSI-SAF are shown in Figs. 16a and 16b, respectively. Both existing SIM products are in good agreement with S1+RCM with correlation coefficients greater than 0.85. Larger speeds are more apparent for S1+RCM with the mean difference (MD) 1.3 km/day for the NSIDC and 0.76 km/day for OSI-SAF for 2020. The root-mean square difference (RMSD) was lower for the NSIDC compared to OSI-SAF at 2.58 km/day and 3.25 km/day, respectively. We note better agreement with NSIDC because of its higher spatial resolution compared to OSI-SAF and the absence of larger ice speeds in NSIDC compared to OSI-SAF due to lower temporal resolution. The overall larger speed~~

~~associated with S1+RCM is most likely the result of higher spatial resolution compared to lower resolution satellite data used in NSIDC and OSI-SAF that is more difficult to track at lower spatial resolution because of temporal decorrelation. Kwok et al. (1998) also noted this problem when comparing SIM from passive microwave with SAR and found it also applies to regions of low ice concentration.~~

~~Although SAR has difficultly tracking sea ice in the vicinity of the marginal ice zone and regions of low concentration, passive microwave has more difficultly. With the high S1+RCM image density available over the marginal ice zone during the melt season (Fig. 6) there was sufficient number of images available during the summer months for S1+RCM to be able to better resolve SIM compared to these existing SIM products with a lower nominal spatial resolution. For example, the spatial distribution of SIM for S1+RCM and NSIDC product in the Beaufort Sea is shown for September 9-15, 2020 in Fig. 17. While larger ice speeds are apparent with S1+RCM, there are also many regions along the marginal ice zone with sea ice concentration (SIC) below 18% that are not detected by NSIDC SIM product.~~

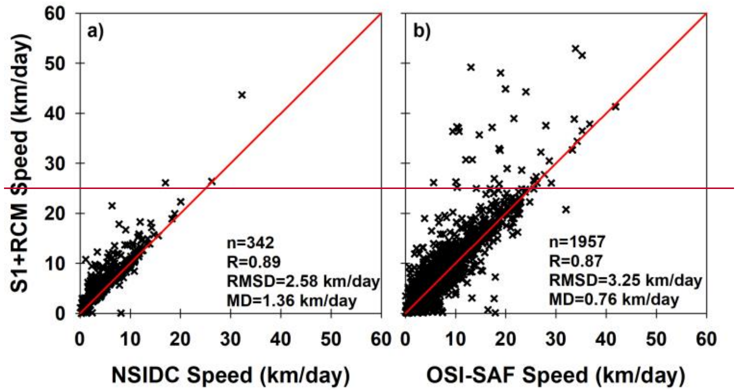

~~**Figure 16. Scatterplots of S1+RCM sea ice motion versus a) National Snow and Ice Data Center (NSIDC) SIM and b) Ocean and Sea Ice Satellite Application Facility (OSI-SAF) sea ice motion. Also shown is the number of samples (n), Pearson's correlation coefficient (R), root-mean square difference (RMSD), and the mean difference (MD).**~~

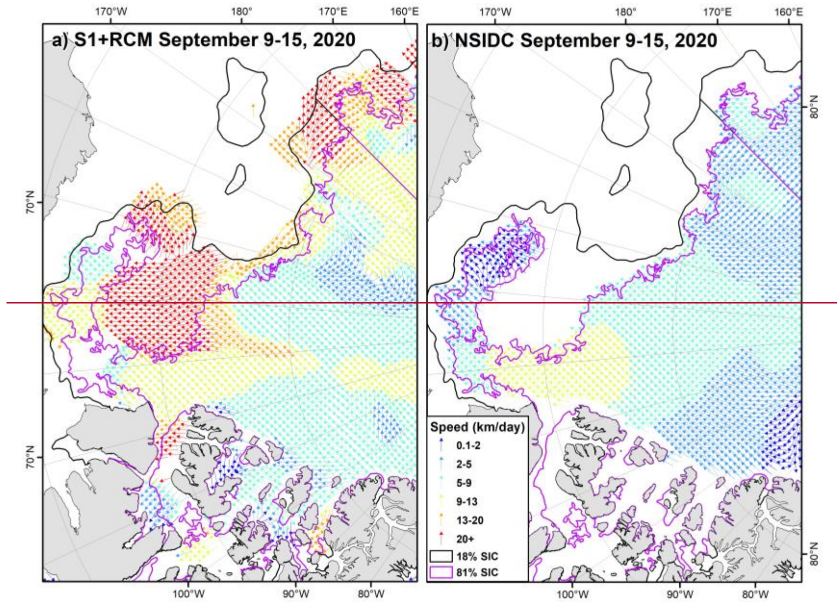

~~**Figure 17. The spatial distribution of a) S1+RCM sea ice motion and b) National Snow and Ice Data Center (NSIDC) sea ice motion in the Beaufort Sea region from September 9-15, 2020. Also shown are the sea ice concentration (SIC) polygons for 18% (black) and 81% (magenta). Note that the white areas in the figure indicate either zero ice motion for the landfast ice or no ice motion information extracted (because of no SAR data, no ice, or no stable ice features).**~~

~~5~~ 7 Conclusions

In this study, we described the ECCC-ASTIS and its application of 135,471 images from 5 SAR satellites from S1 and the RCM to routinely estimate SIM over the large-scale pan-Arctic domain from March 2020 to October 2021. The higher density image coverage of S1+RCM as oppose to just S1 and/or RCM provided more available SAR image pairs over Hudson Bay, Davis Strait, Beaufort Sea, Bering Sea, and the North Pole. S1+RCM SIM covered the majority of the pan-Arctic domain using a spatial resolution of 25 km and temporal resolution of 7-days. 6.25 km 3-day products also were generated and can provide improved spatiotemporal SIM representation in many regions of the pan-Arctic. In particular, the spatial heterogeneity in large-scale S1+RCM SIM at both scales was preserved as well as SIM was able to be resolved within the narrow channels and inlets of the CAA filling a major information gap.

The S1+RCM SIM vectors were compared against buoy estimates from the IABP for both dry and wet ice conditions to assess the performance of the ECCC automated feature tracking algorithm with S1 and RCM imagery. Results indicate an uncertainty of 2.78 km for the former and 3.43 km for the latter and we developed a range of ice speed uncertainties for the S1+RCM SIM products. Comparing the S1+RCM SIM estimates to the existing SIM datasets of NSIDC and OSI SAF revealed that S1+RCM provides larger ice speeds (~4 km/day) confirming the speed bias associated with lower resolution sensors.

The primary purpose of ECCC-ASITS is to routinely deliver SIM information for operational usage within ECCC as well as the scientific community and maritime stakeholders. The data archive is available from March 2020 to October 2021 and updates are produced ad hoc (every few months) but updates are expected to occur more frequently in the near-future. We recognize that the short data record of S1+RCM SIM does not make it well suited for long-term scientific studies. However, the Arctic sea ice is rapidly changing and for recent large-scale process studies or localized studies (e.g. MOSAiC) or regional studies (e.g. CAA) S1+RCM SIM products generated by the ECCC ASTIS can provide more representative SIM estimates than their passive microwave counter-parts. Moreover, the time series of large-scale generated SIM from SAR needs to start now with the currently available and expected continuation of spaceborne SAR missions. The anticipated launch of the NASA-ISRO (NISAR) L&S-band SAR satellite also provides an opportunity to add L-band into the ECCC-ASITS. L-band SAR would be able to provide improved SIM estimates during the melt season compared to C-band (Howell et al., 2018). Even without adding different frequency satellite sensors, the upcoming launch of Sentinel-1C and Sentinel-1D will continue to facilitate the routine generation of large-scale SIM using the ECCC-ASITS from C-band SAR for many years to come.

Future refinements to the ECCC-ASTIS are possible which includes adding the HV channel to complement SIM estimated from HH polarization. Mixing S1 and RCM images offers an opportunity to provide more spatiotemporally refined SIM estimation across the Arctic; however, based on the current image distribution of S1 and RCM it is unlikely to improve spatial coverage as RCM mainly fills in the spatial gaps in S1 coverage. It is also very challenging computationally to produce and work with large-scale SAR derived SIM products at very high spatiotemporal resolution. To that end, mixing sensors at C-band will likely not result in major advances of large-scale automated detected SIM, but it could provide more insight into local scale processes (e.g. fault generation, instantaneous reaction to forcing, inertial oscillations). In this regard, the temporal resolution of mixing S1 and RCM imagery could be pushed to sub-daily in some regions, and we anticipate exploring this option for targeted dense time series applications in the Arctic. While groups such as the Polar Space Task Group aim to improve or refine SAR coverage across the pan-Arctic over the annual cycle, it is unlikely a purely SAR derived SIM product will be able to achieve daily or sub-daily coverage consistently across the pan-Arctic. This has only recently been achieved with passive microwave observations using a swath-to-swath approach (Lavergne et al., 2021). Therefore, it could be worth exploring the complimentary of SIM provided from passive microwave "swath-to-swath" and SIM generated from SAR.

~~In this study we made use of 5 SAR satellites from S1 and the RCM with over 60,000 images to estimate SIM over the large-scale pan-Arctic domain from March to December 2020. The higher density image coverage of S1+RCM as oppose to just S1 and/or RCM provided more available SAR image pairs over Hudson Bay, Davis Strait, Beaufort Sea, Bering Sea, and the North Pole. Results indicated that on average, 4.5 million SIM vectors from S1 and RCM were automatically detected per week for 2020 facilitating the generation of large-scale S1+RCM SIM products. Notable spatial features were apparent (i.e. the Transpolar Drift and the Beaufort Gyre) and the seasonal cycle of sea ice speed exhibited the expected variability with decreases during the melt season and increases into the fall and winter. Moreover, by using an input spatial resolution of 200 m, more spatial heterogeneity in large-scale SIM was preserved as well as SIM was able to be resolved within the narrow channels and inlets across the Arctic. The corresponding S1+RCM SIM vector quality (cross-correlation coefficients) and σ_{SIM} also reflected the seasonal cycle with lower quality vectors and higher σ_{SIM} during the shoulder seasons. Comparing the S1+RCM SIM estimates to the existing SIM datasets of NSIDC and OSI-SAF revealed that S1+RCM provides larger ice~~

~~speeds and detects more vectors in the marginal ice zone. The advantages of detecting SIM from SAR as opposed to passive microwave were ultimately confirmed from a large-scale comparison.~~

~~S1+RCM SIM covered the majority of the pan-Arctic domain from March to December using a spatial resolution of 25 km and temporal resolution of 7-days. However, more consistent spatial coverage was achieved during the melt season given the weekly image density of S1+RCM decreases with decreasing latitude. Continued coordinated efforts by working groups like the Polar Space Task Group are encouraged to improve or refine SAR coverage across the pan-Arctic over the annual cycle. Although, covering the majority of pan-Arctic domain with SIM generated from S1+RCM at spatial resolutions of less than 25 km and temporal resolutions less than 7-days was not consistently possible for 2020, we demonstrated that regional S1+RCM SIM products at higher spatial and temporal resolution are achievable given the weekly image density of S1+RCM.~~

~~The unique nature of the approach to automatically estimate SIM from S1+RCM described in this paper is that future refinements are possible. For instance, we anticipate adding HV channel to complement SIM estimated from HH polarization. Should the timing of when S1 and RCM images acquired and received by ECCC becomes more consistent, we can explore if mixing S1 and RCM images provides most robust pan-Arctic SIM estimation. The anticipated launch of the NASA-ISRO (NISAR) L&S-band SAR satellite also provides an opportunity to add L-band into our SIM processing chain. L-band SAR would be able to provide improved SIM estimates during the melt season compared to C-band (Howell et al., 2018). Even without refining our approach, the upcoming launch of Sentinel-1C and Sentinel-1D will continue to facilitate large-scale SIM from C-band SAR for many years to come.~~

Data availability

The S1 imagery is available at the Copernicus Open Access Hub (https://scihub.copernicus.eu/dhus/#/home) and RCM imagery is available online at Natural Resources Canada's Earth Observation Data Management System (https://www.eodms-sgdot.nrcan-rncan.gc.ca). 62.5 km 2-day sea ice motion from OSI SAF available at: https://osisaf-hl.met.no/osi-405-c-desc. Weekly sea ice motion from the NSIDC Polar Pathfinder available at: https://nsidc.org/data/nsidc-0116. IABP data is available at https://iabp.apl.uw.edu/data.html. Ice charts from the National Ice Center are available at: https://usicecenter.gov/Products/ArcticData. S1+RCM pan-Arctic SIM products generated in this analysis are available at: https://crd-data-donnees-rdc.ec.gc.ca/CPS/products/PanArctic_SIM/.

Author contribution

SELH wrote the manuscript with input from ASK and MB. SELH and MB preformed the analysis. ASK developed the automated sea ice tracking algorithm.

Competing interests

The authors declare that they have no conflict of interest.

References

Agnew, T. A., Le, H., and Hirose, T.: Estimation of large scale sea ice motion from SSM/I 85.5 GHz imagery, Ann. Glaciol., 25, 305– 311, 1997.

Agnew, T., Lambe, A., and Long, D.: Estimating sea ice area flux across the Canadian Arctic Archipelago using enhanced AMSR-E, J. Geophys. Res., 113, C10011, doi:10.1029/2007JC004582, 2008.

Dawson, J., Pizzolato, L., Howell, S. E. L., Copland, L. & Johnston, M. E. Temporal and spatial patterns of ship traffic in the Canadian Arctic from 1990 to 2015. Arctic 71, 15–26 (2018).

Eguíluz, V., Fernández-Gracia, J., Irigoien, X. & Duarte, C. M. A quantitative assessment of Arctic shipping in 2010–2014. Sci. Rep. 6, 30682 (2016).

Emery, W. J., Fowler, C. W., Hawkins, J., and Preller, R. H.: Fram Strait satellite image-derived ice motions, J. Geophys. Res., 96, 4751–4768, 1991.

Fily, M. and Rothrock, D.: Opening and closing of sea ice leads: Digital measurement from synthetic aperture radar, J. Geophys. Res., vol. 95(C1), 789–796. 1990.

Howell, S. E. L., Wohlleben, T., Dabboor, M., Derksen, C., Komarov, A., and Pizzolato, L.: Recent changes in the exchange of sea ice between the Arctic Ocean and the Canadian Arctic Archipelago, J. Geophys. Res., 118, 3595–3607, doi:10.1002/jgrc.20265, 2013.

Howell, S.E.L., Komarov, A.S., Dabboor, M., Montpetit, B., Brady, M., Scharien, R.K., Mahmud, M.S., Nandan, V., Geldsetzer, T., and Yackel, J.J.: Comparing L- and C-band synthetic aperture radar estimates of sea ice motion over different ice regimes, Remote Sensing of Environment, 204, 380-391, https://doi.org/10.1016/j.rse.2017.10.017, 2018.

~~Howell, S.E.L., Small, D., Rohner, C., Mahmud, M.S., Yackel, J.J., and Brady, M.: Estimating melt onset over Arctic sea ice from time series multi-sensor Sentinel-1 and RADARSAT-2 backscatter, Remote Sensing of Environment, doi: 10.1016/j.rse.2019.04.031, 2019.~~

Haarpaintner, J.: Arctic-wide operational sea ice drift from enhanced resolution QuikScat/SeaWinds scatterometry and its validation, IEEE Trans. Geosci. Remote Sens., 44(1), 102–107, 2006.

Komarov, A.S. and Barber, D.G.: Sea ice motion tracking from sequential dual-polarization RADARSAT-2 images. IEEE Trans. Geosci. Remote Sens. 52 (1), 121–136. http://dx.doi.org/10.1109/TGRS.2012.2236845, 2014.

Komarov A.S. and Buehner, M.: Improved retrieval of ice and open water from sequential RADARSAT-2 images. IEEE Trans. Geosci. Remote Sens., 57 (6), 3694-3702, doi: http://dx.doi.org/10.1109/TGRS.2018.2886685, 2019.

Kwok, R., Curlander, J., McConnell, R., and Pang, S.: An ice-motion tracking system at the Alaska SAR facility, IEEE J. Ocean. Eng., 15(1), 44–54, 1990.

Kwok, R., Schweiger, A., Rothrock, D.A., Pang, S., and Kottmeier, C.: Sea ice motion from satellite passive microwave data assessed with ERS SAR and buoy data, J. Geophys. Res., 103, 8191–8214, 1998.

Kwok, R.: Annual cycles of multiyear sea ice coverage of the Arctic Ocean: 1999–2003, J. Geophys. Res., 109, C11004, doi:10.1029/2003JC002238, 2004.

Kwok, R.: Exchange of sea ice between the Arctic Ocean and the Canadian Arctic Archipelago, Geophys. Res. Lett., 33, L16501, doi:10.1029/2006GL027094, 2006.

Kwok, R.: Outflow of Arctic Ocean Sea Ice into the Greenland and Barents Seas: 1979–2007, Journal of Climate, 22, 2438–2457, DOI: https://doi.org/10.1175/2008JCLI2819.1, 2009.

Kwok, R., Spreen, G., and Pang, S.: Arctic sea ice circulation and drift speed: Decadal trends and ocean currents, J. Geophys. Res. Oceans, 118, 2408–2425, doi:10.1002/jgrc.20191, 2013.

Lavergne, T., Eastwood, S., Teffah, Z., Schyberg, H., and Breivik, L.-A: Sea ice motion from low-resolution satellite sensors: An alternative method and its validation in the Arctic, J. Geophys. Res., 115, C10032, doi:10.1029/2009JC005958, 2010.

Lavergne, T., Piñol Solé, M., Down, E., and Donlon, C.: Towards a swath-to-swath sea-ice drift product for the Copernicus Imaging Microwave Radiometer mission, The Cryosphere, 15, 3681–3698, https://doi.org/10.5194/tc-15-3681-2021, 2021.

Melling, H.: Sea ice of the northern Canadian Arctic Archipelago, J. Geophys. Res., 107(C11), 3181, doi:10.1029/2001JC001102, 2002

Moore, G. W. K., Schweiger, A., Zhang, J., and Steele, M.: Spatiotemporal variability of sea ice in the Arctic's Last Ice Area. Geophysical Research Letters, 46, https://doi.org/10.1029/2019GL083722, 2019.

Moore, G.W.K., Howell, S.E.L., Brady, M., McNeil, K., and Xu, X: Anomalous collapses of Nares Strait ice arches leads to enhanced export of Arctic sea ice, Nature Communications, 12, 1, https://doi.org/10.1038/s41467-020-20314-w, 2021a.

Moore, G. W. K., Howell, S. E. L., & Brady, M.: First observations of a transient polynya in the Last Ice Area north of Ellesmere Island. Geophysical Research Letters, 48, e2021GL095099. https://doi.org/10.1029/2021GL095099, 2021b.

Mudryk, L.R., Dawson, J., Howell, S.E.L. Derksen, C., Zagon, T.A., and M. Brady: Impact of 1, 2 and 4 °C of global warming on ship navigation in the Canadian Arctic. Nat. Clim. Chang. 11, 673–679. https://doi.org/10.1038/s41558-021-01087-6, 2021.

Notz, D., and Stroeve, J.: Observed Arctic sea-ice loss directly follows anthropogenic CO2 emission, Science, 354(6313),747-750, DOI: 10.1126/science.aag2345, 2016.

Rampal, P., Weiss, J., and Marsan, D: Positive trend in the mean speed and deformation rate of Arctic sea ice, 1979–2007, J. Geophys. Res., 114, C05013, doi:10.1029/2008JC005066, 2009.

Rigor, I. G., Wallace, J.M., and Colony, R.L.: On the response of sea ice to the Arctic Oscillation, J. Clim., 15(18), 2546–2663, 2002.

~~Small, D., Rohner, C., Miranda, N., Rüetschi, M., and Schaepman, M.E.: Wide-Area Analysis-Ready Radar Backscatter Composites, IEEE Transactions on Geoscience and Remote Sensing, doi: 10.1109/TGRS.2021.3055562, 2021.~~

Thompson, A. A.: Overview of the RADARSAT Constellation Mission. Canadian Journal of Remote Sensing, 41(5), 401-407. https://doi.org/10.1080/07038992.2015.1104633, 2015.

Thorndike, A. S. and Colony, R.: Sea ice motion in response to geostrophic winds, J. Geophys. Res., 87(C8), 5845– 5852, doi:10.1029/JC087iC08p05845, 1982.

Torres, R., Snoeij, P., Geudtner, D., Bibby, D., Davidson, M., Attema, E., … Rostan, F.: GMES Sentinel-1 mission. Remote Sensing of Environment, 120, 9–24. https://doi.org/10.1016/j.rse.2011.05.028, 2012.

Tschudi, M. A., Meier, W. N., and Stewart, J. S.: An enhancement to sea ice motion and age products at the National Snow and Ice Data Center (NSIDC), The Cryosphere, 14, 1519–1536, https://doi.org/10.5194/tc-14-1519-2020, 2020.

Wagner, P.M., Hughes, N., Bourbonnais, P., Stroeve, J., Rabenstein, L., Bhatt, U., Little, J., Wiggins H., and Fleming, A: Sea-ice information and forecast needs for industry maritime stakeholders, Polar Geography, 43:2-3, 160-187, DOI: 10.1080/1088937X.2020.1766592, 2020.